GEOMETRY, ANALYSIS, AND MORPHOGENESIS: PROBLEMS AND PROSPECTS

MARTA LEWICKA AND L. MAHADEVAN

Abstract. The remarkable range of biological forms in and around us, such as the undulating shape of a leaf or flower in the garden, the coils in our gut, or the folds in our brain, raise a number of questions at the interface of biology, physics, and mathematics. How might these shapes be predicted, and how can they eventually be designed? We review our current understanding of this problem, which brings together analysis, geometry, and mechanics in the description of the morphogenesis of low-dimensional objects. Starting from the view that shape is the consequence of metric frustration in an ambient space, we examine the links between the classical Nash embedding problem and biological morphogenesis. Then, motivated by a range of experimental observations and numerical computations, we revisit known rigorous results on curvature-driven patterning of thin elastic films, especially the asymptotic behaviors of the solutions as the (scaled) thickness becomes vanishingly small and the local curvature can become large. Along the way, we discuss open problems that include those in mathematical modeling and analysis along with questions driven by the allure of being able to tame soft surfaces for applications in science and engineering.

1. Introduction

A walk in the garden, a visit to the zoo, or watching a nature documentary reminds us of the remarkable range of living forms on our planet. How these shapes come to be is a question that has interested scientists for eons, and yet it is only over the last century that we have finally begun to grapple with the framework for morphogenesis, a subject that naturally brings together biologists, physicists, and mathematicians. This confluence of approaches is the basis for a book, equally lauded for both its substance and its scientific style, D'Arcy Thompson's opus, *On growth and form* [116], where the author says:

> An organism is so complex a thing, and growth so complex a phenomenon, that for growth to be so uniform and constant in all the parts as to keep the whole shape unchanged would indeed be an unlikely and an unusual circumstance. Rates vary, proportions change, and the whole configuration alters accordingly.

From both mathematical and mechanical perspectives, this suggests a simple principle: differential growth in a body leads to residual strains that will generically result in changes in the shape of a tissue, organ, or body. Surprisingly then, it is only recently that this principle has been taken up seriously by both experimental and theoretical communities as a viable candidate for patterning at the cellular and tissue level, perhaps because of the dual difficulty of measuring and of calculating the mechanical causes and consequences of these effects. Nevertheless, with an increasing number of testable predictions and high throughput imaging in space-time, this geometric and mechanical perspective on morphogenesis has begun to be viewed as a complement to the biochemical aspects of morphogenesis, as famously exemplified by the work of Alan Turing in his prescient paper, *The chemical basis for morphogenesis* [119]. It is worth pointing out that differential diffusion and growth are only parts of an entire spectrum of mechanisms involved in morphogenesis that include differential adhesion, differential mobility, differential affinity, and differential activity, all of which we must eventually come to grips with to truly understand the development and evolution of biological shape.

In this review, we consider the interplay between geometry, analysis, and morphogenesis of thin surfaces driven by three motivations: the allure of quantifying the aesthetic seen in examples such as flowers, the hope of explaining the origin of shape in biological systems, and the promise of mimicking them in artificial systems [64, 106]. While these issues also arise in three-dimensional tissues in such examples as the folding of the brain [113, 114] or the looping of the gut [105, 111], the separation of scales in slender structures that grow in the plane and out of it links the physical problem of growing elastic films to the geometrical problem of determining a slowly evolving approximately two-dimensional film in three dimensions. Indeed, as we will see, many of the questions we review here are related to a classical theme in differential geometry—that of embedding a shape with a given metric in a space of possibly different dimension [95, 96], and eventually that of designing the metric to achieve any given shape. However, the goal now is not only to state the conditions when it might be done (or not) but also to determine the resulting shapes in terms of an appropriate mechanical theory and to understand the limiting behaviors of the solutions as a function of the geometric parameters.

The outline of this paper is as follows. Starting from the view that shape is the consequence of metric frustration in an ambient space, in section 2 we describe the background and objectives of non-Euclidean elasticity formalism as well as present an example of growth equations in this context. In section 3 we examine the links between the classical Nash embedding problem and biological morphogenesis. Then, motivated by a range of experimental observations and numerical computations, we revisit known rigorous results on curvature-driven patterning of thin elastic films in section 4, where we also offer a new estimate regarding the scaling of non-Euclidean energies from convex integration. In section 5, we focus on the asymptotic behaviors of the solutions as the (scaled) thickness of the films becomes vanishingly small and the local curvature can become large. In section 6 we digress to consider the weak prestrains and the related Monge–Ampère constrained energies. In section 7, the complete range of results is compared with the hierarchy of classical geometrically nonlinear theories for elastic plates and shells without prestrain. Along the way and particularly in section 8, we discuss open mathematical problems and future research directions.
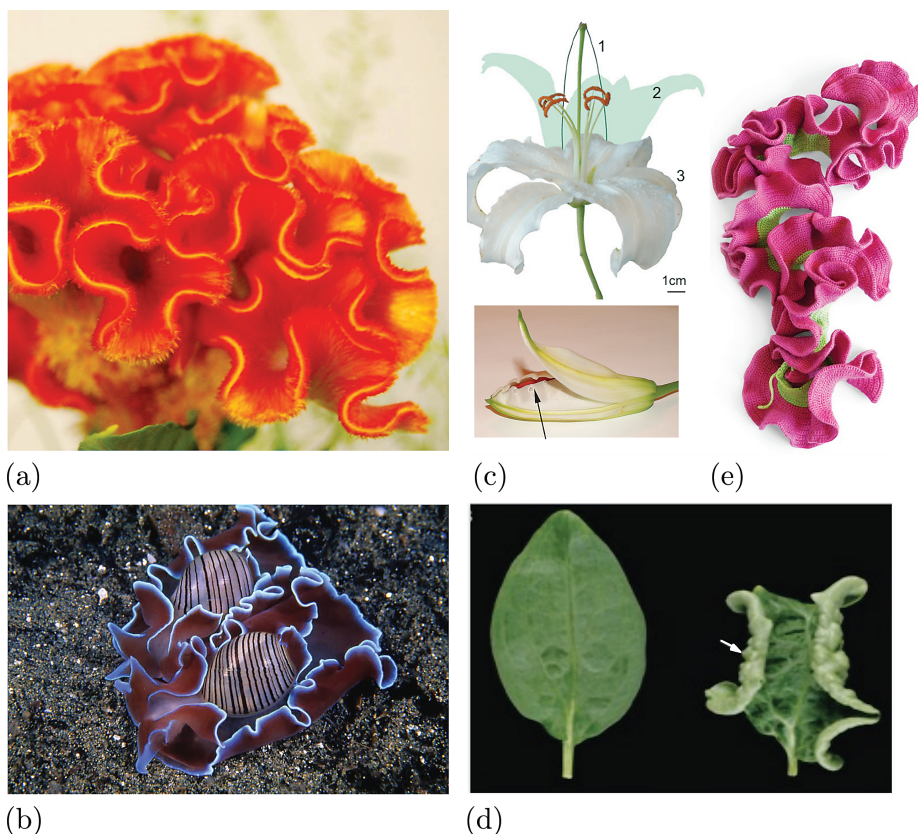
FIGURE 1. Patterns in a range of systems in terrestrial and aquatic environments show the myriad forms that reflect the consequence of inhomogeneous growth of a thin sheet: the impossibility of embedding an arbitrary biological growth metric coupled with the constraint of minimizing an elastic energy leads to frustration embodied as shape. The examples shown are (a) a terrestrial cockscomb flower, (b) a marine nudibranch sea-slug, (c) a lily flower in its bud and opened states [90], (d) a normal and mutant snapdragon leaf, (e) a crocheted scarf. All these are frustrated embeddings of a hyperbolic metric into $\mathbb{R}^3$. (This figure is available via Creative Commons Attribution–NonCommercial–NoDerivatives 4.0 International license.)

2. Non-Euclidean elasticity and an example of growth equations

An inexpensive surgical experiment serves as a clue to the biological processes at work in determining shape: if one takes a sharp knife and cuts a long, rippled leaf into narrow strips parallel to the midrib, the strips flatten out when "freed" from the constraints of being contiguous with each other. This suggests that the shape is the result of geometric frustration and feedback, driven by the twin effects

of embedding a non-Euclidean metric due to inhomogeneous growth and of minimizing an elastic energy that selects the particular observed shape. Experiments confirm the generality of this idea in a variety of situations, ranging from undulating submarine avascular algal blades to saddle-shaped, coiled, or edge-rippled leaves of many terrestrial plants [66, 89]. Understanding the origin of the morphologies of slender structures as a consequence of either their growth or the constraints imposed by external forces, requires a mathematical theory for how shape is generated by inhomogeneous growth in a tissue.

2.1. **Non-Euclidean elasticity.** Biological growth arises from changes in four fields: cell number, size, shape, and motion, all of which conspire to determine the local metric, which in general will not be compatible with the existence of an isometric immersion. For simplicity, growth is often coarse-grained by averaging over cellular details, thus ignoring microscopic structure due to cellular polarity, orientation (nematic order), anisotropy, etc. While recent work has begun to address these more challenging questions [93, 122], we limit our review to the case of homogeneous, isotropic thin growing bodies. This has proceeded along three parallel paths, all leading to a set of coupled hyperelliptic PDEs that follow from a variational principle:

- by using the differential geometry of surfaces as a starting point to determine a plausible class of elastic energies written in terms of the first and second fundamental forms or their discrete analogues and deviations from some natural state [49];
- by drawing on an analogy between growth and thermoelasticity [91] and plasticity [73], since they both drive changes in the local metric tensor and the second fundamental form, and by using this to build an energy functional whose local minima determines shape;
- by starting from a three-dimensional theory for a growing elastic body with geometrically incompatible growth tensors, driving the changes of the first and second fundamental forms of a two-dimensional surface embedded in three dimensions [7, 27].

The resulting shape can be seen as a consequence of the heterogeneous incompatibility of strains that leads to geometric (and energetic) frustration. This coupling between residual strain and shape implies an energetic formulation of *non-Euclidean elasticity* that attempts to minimize an appropriate energy associated with the frustration between the induced and intrinsic geometries. Within this framework, a few different types of problems may be posed:

- questions about the nature of the (regular and singular) solutions that arise;
- questions about their connection to experimental observations;
- problems related to the limiting behavior of the solutions and their associated energies in the limit of small (scaled) thickness;
- questions about identifying the form of feedback laws linking growth to shape that lead to the self-regulated reproducible forms seen in nature;
- problems in formulating inverse problems in the context of shaping sheets for function.

2.2. **An example of growth equations.** To get a glimpse of the analytical struc-
tures to be investigated, we begin by writing down a minimal theory that couples
growth to the shape of a thin lamina of uniform thickness [7,89,91], now generalized
to account for differential growth:

$$\Delta(\operatorname{tr}\boldsymbol{\sigma}) + \frac{\alpha}{2}\det\boldsymbol{\kappa} = -\alpha\Delta(\operatorname{tr}\mathbf{s}),$$

(2.1)

$$\beta\Delta(\operatorname{tr}\boldsymbol{\kappa}) - \operatorname{tr}(\boldsymbol{\sigma}\boldsymbol{\kappa}) = -\beta\Delta(\operatorname{tr}\mathbf{b}).$$

Here, Δ is the two-dimensional Laplace–Beltrami operator, $\boldsymbol{\sigma}$ is the two-dimensional
depth-averaged stress tensor, and $\boldsymbol{\kappa}$ is the curvature tensor. The scalar coefficients
α and β characterize the elastic moduli of the sheet, assumed to be made of a linear
isotropic material: α is the resistance to stretching (and shearing) in the plane, and
β is the resistance to bending out of the plane. The right-hand side of (2.1) quan-
tifies the source that drives in-plane differential growth due to a prescribed metric
tensor $\mathbf{s}$, and the out-of-plane differential growth gradient across the thickness due
to a prescribed second fundamental form (a curvature tensor) $\mathbf{b}$.

The first equation in the system (2.1) corresponds to the incompatibility of the
in-plane strain due to both the Gauss curvature and the additional contribution
from in-plane differential growth, and it is a geometric compatibility relation. The
second equation in system (2.1) is a manifestation of force balance in the out-of-
plane direction due to the in-plane stresses in the curved shell and to the growth
curvature tensor associated with transverse gradients that leads to an effective
normal pressure. We observe that $\beta/\alpha = \mathcal{O}(h^2)$, where h is the thickness of the
tissue, so there is a natural small parameter in the problem $a = h/L \ll 1$, where
L is the lateral size of the system. The nonlinear hyperelliptic equations (2.1)
need to be complemented with an appropriate set of boundary conditions on some
combination of the displacements, stresses, and their derivatives. However, it is
not even clear if and when it is possible to realize reasonable physical surfaces for
arbitrarily prescribed tensors $\mathbf{s}, \mathbf{b}$, and so one must resort to a range of approximate
methods to determine the behavior of the solutions in general.

There are two large classes of problems associated with the appearance of fine
scales or sharp localized conical features, and they are characterized by two distin-
guished limits of (2.1). These correspond to the situation when either the in-plane
stress is relatively large or when it is relatively small. In the first case, when $|\boldsymbol{\sigma}| \sim \alpha$,
i.e., the case where stretching dominates, one can rescale equations (2.1) so that
they yield the singularly perturbed limit:

$$\Delta(\operatorname{tr}\boldsymbol{\sigma}) + \frac{1}{2}\det\boldsymbol{\kappa} = -\Delta(\operatorname{tr}\mathbf{s}),$$

(2.2)

$$a^2\Delta(\operatorname{tr}\boldsymbol{\kappa}) - \operatorname{tr}(\boldsymbol{\sigma}\boldsymbol{\kappa}) = -a^2\Delta(\operatorname{tr}\mathbf{b}).$$

As $a^2 \to 0$, at leading order, the second of the equations above implies $\operatorname{tr}(\boldsymbol{\sigma}\boldsymbol{\kappa}) =$
0, which has a simple geometric interpretation. Namely, the stress-scaled mean
curvature vanishes, which is an interesting generalization of the Plateau–Lagrange
problem for minimal surfaces. Then, system (2.2) describes a finely decorated
minimal surface, where wrinkling patterns appear in regions with a sufficiently
negative stress.

In the second case, when the in-plane stress is relatively small $|\boldsymbol{\sigma}| \sim \alpha a^2$, i.e., the
case when bending dominates, one can rescale (2.1) to obtain a different singularly

perturbed limit:

$$(2.3) \qquad a^2 \Delta(\operatorname{tr} \boldsymbol{\sigma}) + \frac{1}{2} \det \boldsymbol{\kappa} = -\Delta(\operatorname{tr} \mathbf{s}),$$
$$\Delta(\operatorname{tr} \boldsymbol{\kappa}) - \operatorname{tr}(\boldsymbol{\sigma}\boldsymbol{\kappa}) = -\Delta(\operatorname{tr} \mathbf{b}).$$

As $a^2 \to 0$, at leading order the first of the equations above yields $\det \boldsymbol{\kappa} = -2\Delta(\operatorname{tr} \mathbf{s})$, which can be seen as a Monge–Ampère type equation for the Gauss curvature. Then, system (2.3) describes a spontaneously crumpled, freely growing sheet with conical and ridge-like singularities, similar to the result of many a failed calculation that ends up in the recycling bin.

Adding the growth terms in (2.1) is however only part of the biological picture, since in general there is likely to be feedback; i.e., just as growth leads to shape, shape (and residual strain) can change the growth patterns. Then, the growth tensors $\mathbf{s}, \mathbf{b}$ must themselves be coupled to the shape of the sheet via additional (dynamical) equations.

Open Problem 2.1. The above description follows the one-way coupling of growth to shape and ignores the feedback from the residual strain. It is known that biological mechanisms inhibit cell growth if the cell experiences sufficient external pressure. Although there are proposals for how shape couples back to growth, this remains a largely open question of much current interest in biology, and we will return to this briefly in the concluding sections.

3. Shape from geometric frustration in growing laminae

The variety of forms seen in the three-dimensional shapes of leaves or flowers, reflects their developmental and evolutionary history and the physical processes that shape them, posing many questions at the nexus of biology, physics, and mathematics. From a biological perspective, it is known that genetic mutants responsible for differential cell proliferation lead to a range of leaf shapes [97, 125]. From a physical perspective, stresses induced by external loads lead to phenotypic plasticity in algal blades that switch between long, narrow blade-like shapes in rapid flow to broader undulating shapes in slow flow [66]. Similar questions arise from observations of a blooming flower—long an inspiration for art and poetry, but seemingly not so from scientific perspectives. When a flower blossoms, its petals change curvature on a time scale of a few hours, consistent with the idea that these movements are driven by cellular processes. In flowers that bloom once, differential cell proliferation is the dominant mode of growth, while in those that open and close repeatedly, cell elongation plays an important role.

Although proposed explanations for petal movements posit a difference in growth rate of its two sides (surfaces) or an active role for the midribs, experimental, theoretical, and computational studies [90] have shown that the change of the shape of a lamina is due to excess growth of the margins relative to the center (see Figure 1). Indeed, there is now ample evidence of how relative growth leads to variations in shape in such contexts as leaves, flowers, micro-organisms (i.e., euglenids), swelling sheets of gels, 4d printed structures etc. [3, 8, 36, 47, 62, 63, 107, 124]. A particularly striking example is that of the formation of self-similar wrinkled structures as shown in the example of a kale leaf in Figure 2. A demonstration of the same phenomenon with everyday materials is also shown in Figure 2—when a garbage bag is torn, its edge shows multiple generations of wrinkles [106].
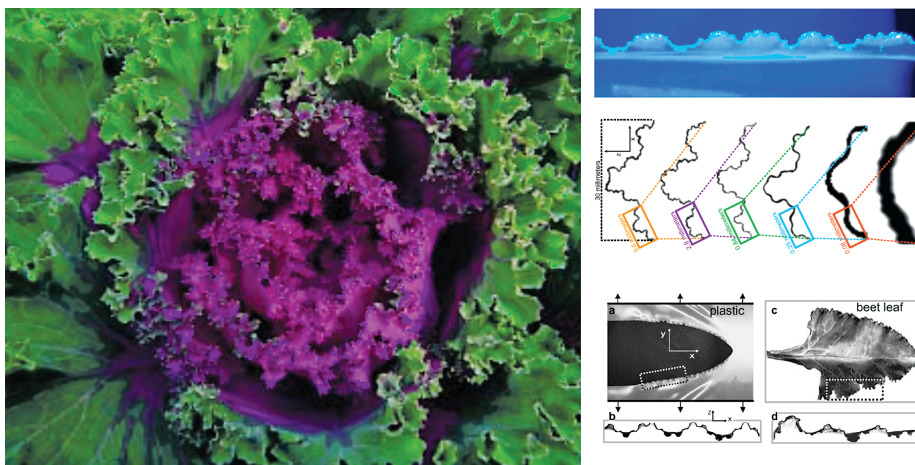
FIGURE 2. The image of purple kale on the left shows that the edges of the leaf are wrinkled hierarchically as the thickness of the kale reduces. This can be captured [23] in a simple tearing experiment of a garbage bag—the tearing edge thins, is plastically deformed, and thus wrinkles. There is a clear hierarchy seen. The images on the right show the analogy between the mechanically deformed edge of the torn sheet and the edge of a beet leaf. (The figure on the left is available via Creative Commons Attribution–NonCommercial–NoDerivatives 4.0 International license. The figure on the right appeared in [23], Cerda, Ravi-Chandar, and Mahadevan, *Wrinkling of a stretched elastic sheet*, Nature, **419** (2002), 579; © 2002, Springer Nature.)

3.1. **The setup.** The experimental observations described above suggest a common mathematical framework for understanding the origin of shape: an elastic three-dimensional body Ω seeks to realize a configuration with a prescribed Riemann metric g by means of an isometric immersion. The deviation from or inability to reach such a state, is due to a combination of geometric incompatibility and the requirements of elastic energy minimization. Borrowing from the theory of finite plasticity [73], where a multiplicative decomposition of the deformation gradient into an elastic and a plastic use was postulated, a similar hypothesis was suggested for growth [104], with the underlying hypothesis of the presence of a reference configuration Ω with respect to which all displacements are measured.

Let $g : \Omega \to \mathbb{R}^{3\times3}_{\mathrm{sym},>}$ be a smooth Romanian metric, given on an open, bounded domain $\Omega \subset \mathbb{R}^3$, and let $u : \Omega \to \mathbb{R}^3$ be an immersion that corresponds to the elastic body. Excluding nonphysical deformations that change the orientation in any neighborhood of the immersion, a natural way to pose the question of the origin of shape is by postulating that it arises from a variational principle that minimizes an elastic energy $\mathcal{E}(u)$ which measures how far a given u is from being an orientation-preserving realization of g. Equivalently, $\mathcal{E}(u)$ quantifies the total pointwise deviation of ∇u from $g^{1/2}$, modulo orientation-preserving rotations that do not cost any energy. The infamy of $\mathcal{E}$ in absence of any forces or boundary conditions is

then indeed strictly positive for a non-Euclidean g, pointing to existence of residual strain.

Since the matrix $g(x)$ is symmetric and positive definite, it possesses a unique symmetric, positive definite square root $A(x) = g(x)^{1/2} \in \mathbb{R}^{3\times 3}_{\text{sym},>}$ which corresponds to the growth prestrain. This allows us to define an energy,

$$(3.1) \qquad \mathcal{E}(u) = \int_\Omega W\left((\nabla u)A^{-1}\right) \, \mathrm{d}x \qquad \forall u \in W^{1,2}(\Omega, \mathbb{R}^3),$$

where the energy density $W : \mathbb{R}^{3\times 3} \to [0, \infty]$ obeys the principles of material frame invariance (with respect to the special orthogonal group of proper rotations $SO(3)$), normalization, nondegeneracy, and material consistency valid for all $F \in \mathbb{R}^{3\times 3}$ and all $R \in SO(3)$,

$$(3.2) \qquad \begin{aligned} & W(RF) = W(F), \qquad W(\mathrm{Id}_3) = 0, \qquad W(F) \geq c \ \mathrm{dist}^2(F, SO(3)), \\ & W(F) \to +\infty \quad \text{as } \det F \to 0+, \quad \text{and} \quad \forall \det F \leq 0 \quad W(F) = +\infty. \end{aligned}$$

These models,[1] corresponding to a range of hyperelastic energy functionals that approximate the behavior of a large class of elastomeric materials, are consistent with microscopic derivations based on statistical mechanics, and they naturally reduce to classical linear elasticity when $|(F^T F)^{1/2} - \mathrm{Id}| \ll 1$. Minimizing the energy (3.1) is thus a prescription for shape and may be defined naturally in terms of the energetic cost of deviating from an isometric immersion.

3.2. **Isometric immersions and residual stress.** The model in (3.1) assumes that the 3d elastic body Ω seeks to realize a configuration with a prescribed Riemannian metric g, through minimizing the energy that is determined by the elastic part $F_e = (\nabla u)A^{-1}$ of the deformation gradient ∇u. Observe that $W(F_e) = 0$ if and only if $F_e \in SO(3)$ in ω, or equivalently when:

$$(\nabla u)^T \nabla u = g \quad \text{and} \quad \det \nabla u > 0 \quad \text{in } \omega,$$

Further, any $u \in W^{1,2}(\Omega, \mathbb{R}^3)$ that satisfies the above must automatically be smooth. Indeed, writing $\nabla u = Rg^{1/2}$ for some rotation field $R : \Omega \to SO(3)$, it follows that $u \in W^{1,\infty}$ and so $\mathrm{div}\left(\mathrm{cof} \, \nabla u\right) = 0$ holds, in the sense of distributions.[2] Further, we have

$$(3.3) \qquad \begin{aligned} \mathrm{cof} \, \nabla u &= \mathrm{cof}(Rg^{1/2}) = \det(Rg^{1/2})\left(Rg^{1/2}\right)^{T,-1} \\ &= \sqrt{\det g}\left(Rg^{-1/2}\right) = \sqrt{\det g}\left((\nabla u)g^{-1}\right). \end{aligned}$$

It follows that each of the three scalar components of u is harmonic with respect to the Laplace–Beltrami operator Δ_g, and thus u must be smooth:

$$0 = \mathrm{div}\left(\mathrm{cof} \, \nabla u\right) = \mathrm{div}\left((\sqrt{\det g})(\nabla u)g^{-1}\right) = \sqrt{\det g} \cdot \left[\Delta_g u^m\right]_{m=1}^3.$$

Thus, $\mathcal{E}(u) = 0$ if and only if the deformation u is an orientation-preserving isometric immersion of g into $\mathbb{R}^3$. Such smooth (local) immersion exists [112, Vol. II, Chapter 4] and is automatically unique up to rigid motions of $\mathbb{R}^3$, if and only if the Riemann curvature tensor $[\mathcal{R}_{ij,kl}]_{i,j,k,l=1\cdots 3}$ of g vanishes identically throughout Ω.

---

[1]Examples of W satisfying these conditions are $W_1(F) = |(F^T F)^{1/2} - \mathrm{Id}|^2 + |\log \det F|^q$ or $W_2(F) = |(F^T F)^{1/2} - \mathrm{Id}|^2 + |(\det F)^{-1} - 1|^q$ for $\det F > 0$, where $q > 1$ and $W_{1,2}$ equal $+\infty$ if $\det F \leq 0$.

[2]The divergence of a matrix field is taken row-wise.

It is instructive to point out that one could define the energy as the difference between the prescribed metric g and the pull-back metric of u on Ω:

$$I(u) = \int_\Omega |(\nabla u)^T \nabla u - g|^2 \; \mathrm{d}x.$$

From a variational point of view, the formulation above does not capture an essential aspect of the physics, namely that thin laminae resist bending deformations that are a consequence of the extrinsic geometry, and thus depend on the mean curvature as well. Indeed, the functional I always minimizes to 0 because there always exists a Lipschitz isometric immersion $u \in W^{1,\infty}(\Omega, \mathbb{R}^3)$ of g, for which $I(u) = 0$. If $\mathcal{R}_{ij,kl}(x) \neq 0$ for some $x \in \Omega$, then such u must have a *folding structure* [50] around x; it cannot be orientation preserving (or reversing) in any open neighborhood of x. Perhaps even more surprisingly, the set of such Lipschitz isometric immersions is dense in the set of short immersions as for every $u_0 \in \mathcal{C}^1(\bar{\Omega}, \mathbb{R}^3)$ satisfying $(\nabla u_0)^T \nabla u_0 < g$,[3] there exists a sequence $\{u_n \in W^{1,\infty}(\Omega, \mathbb{R}^3)\}_{n\to\infty}$ satisfying

$$I(u_n) = 0 \quad \text{and} \quad \|u_n - u_0\|_{\mathcal{C}(\Omega)} \to 0 \quad \text{as} \ \ n \to \infty.$$

The above statement is an example of the *h-principle* in differential geometry, and it follows through the method of convex integration (the Nash–Kuiper scheme), to which we come back in the following sections. An intuitive example in dimension 1 is shown in Figure 3. Setting $g \equiv 1$ on $\Omega = (-1, 1) \subset \mathbb{R}^1$, it is easily seen that any $u_0 : (-1, 1) \to \mathbb{R}$ with Lipschitz constant less than 1 can be uniformly approximated by u_n having the form of a zigzag, where $|u'_n| = 1$.
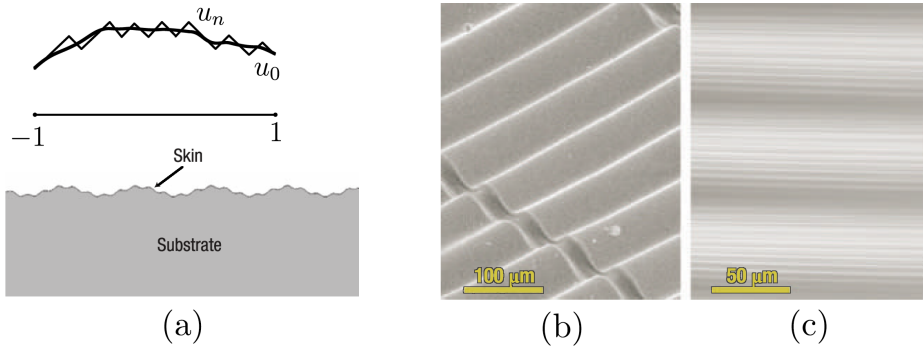

FIGURE 3. (a) A short map approximation of u_0 (darker line) by a zigzag u_n with $u'_n = \pm 1$. (b) A computational realization of hierarchical wrinkles that arise when a thin stiff film is coated atop a soft substrate and the system is then subject to a reduction in temperature that leads to differential shrinkage [39]. (c) An experimental realization of the hierarchical wrinkles that shows two (of a total of six) generations of wrinkles. The three examples serve to link convex integration to models and experiments in materials science [39]. (This figure appeared in [39], Efimenko, Rackaitis, Manias, Vaziri, Mahadevan, and Genzer, *Self-similar nested wrinkling patterns in skins*, Nature–Materials, **4** (2005), 293–297; © 2005, Springer Nature.)

---

[3]That is, the matrix $g(x) - \nabla u_0(x)^T \nabla u_0(x)$ is positive definite at each $x \in \omega$.

Regarding the energy $\mathcal{E}$ in (3.1), in [85] it has been proved that $\inf \mathcal{E} > 0$ for any g with no orientation-preserving isometric immersion. This results in the dichotomy: either g and $\mathcal{E}$ are, by a smooth change of variable, equivalent to the case with $g = \mathrm{Id}_3$ and $\min \mathcal{E} = 0$, or otherwise the zero energy level cannot be achieved through a sequence of weakly regular $W^{1,2}$ deformations. The latter case points to existence of *residual strain at free equilibria*.

Proposition 3.1 ([85]). *If $[\mathcal{R}_{ij,kl}] \not\equiv 0$ in Ω, then $\inf \big\{ \mathcal{E}(u); \ u \in W^{1,2}(\Omega, \mathbb{R}^3) \big\} > 0$.*

Sketch of proof. Assume, by contradiction, that $\mathcal{E}(u_n) \to 0$ along some sequence $\{u_n \in W^{1,2}(\Omega, \mathbb{R}^3)\}_{n \to \infty}$. By truncation and approximation in Sobolev spaces, we may, without loss of generality, assume that each u_n is Lipschitz with a uniform Lipschitz constant M. Decompose $u_n = z_n + w_n$ as a sum of a deformation that is clamped at the boundary,

$$[\Delta_g z_n^m]_{m=1}^3 = [\Delta_g u_n^m]_{m=1}^3 \quad \text{in } \Omega, \qquad z_n = 0 \quad \text{on } \partial\Omega,$$

and a harmonic correction, $[\Delta_g w_n^m]_{m=1}^3 = 0$ in Ω, with $w_n = u_n$ on $\partial\Omega$. Observe that

$$\int_\Omega \big\langle (\sqrt{\det g}) \nabla z_n g^{-1} : \nabla z_n \big\rangle \, \mathrm{d}x = \int_\Omega \big\langle (\sqrt{\det g}) \nabla u_n g^{-1} : \nabla z_n \big\rangle \, \mathrm{d}x$$

$$= \int_\Omega \big\langle (\sqrt{\det g}) \nabla u_n g^{-1} : \nabla z_n \big\rangle - \big\langle \mathrm{cof} \ \nabla u_n : \nabla z_n \big\rangle \, \mathrm{d}x$$

$$\leq \|\nabla z_n\|_{L^2} \big\| (\sqrt{\det g}) \nabla u_n g^{-1} - \mathrm{cof} \ \nabla u_n \big\|_{L^2},$$

where the first equality follows by $z_n = 0$ on $\partial\Omega$, as $\mathrm{div} \big((\sqrt{\det g}) (\nabla u) g^{-1} \big) = \sqrt{\det g} \big[\Delta_g u^m\big]_{m=1}^3$, while the second by $\mathrm{div}(\mathrm{cof} \ \nabla u) = 0$. The left-hand side is also equivalent to $\|\nabla z_n\|_{L^2}^2$, so

$$(3.4) \qquad \|\nabla z_n\|_{L^2} \leq C \big\| (\sqrt{\det g}) \nabla u_n g^{-1} - \mathrm{cof} \ \nabla u_n \big\|_{L^2} \leq C_M \mathcal{E}(u_n)^{1/2} \to 0.$$

Above, we used (3.3) which ensures vanishing of the expression under the norm when $(\nabla u_n) A^{-1} \in SO(3)$, together with Lipschitz continuity of the operator in the integral expression for $\mathcal{E}$. In particular, we get that both sequences $\{\nabla z_n\}_{n \to \infty}$ and $\{\nabla w_n\}_{n \to \infty}$ are bounded in L^2.

Since $\{w_n\}$ are harmonic, this further implies that ∇u_n converges, up to a subsequence, in L^2_{loc} to some ∇u. Then by (3.4) $\nabla u_n \to \nabla u$, which yields $\mathcal{E}(u) = 0$, and ends the proof. $\square$

Open Problem 3.2. In the above context, prove that $\inf \mathcal{E}$ as in Proposition 3.1 is equivalent to $\|[\mathcal{R}_{ij,kl}]\|_{H^{-2}}^2$, up to multiplicative constants depending on Ω and W but not on g. The case of $\Omega \subset \mathbb{R}^2$ and $\mathcal{R}$ replaced by the Gaussian curvature has been considered in [72].

4. Microstructural patterning of thin elastic prestrained films

Inspired partly by biological observations of growth-induced patterning in thin sheets and the promise of engineering applications, various techniques have been invented for the construction of self-actuating elastic sheets with prescribed target metrics. The materials typically involve the use of gels that respond to pH, humidity, temperature, and other stimuli [115], and that result in the formation of complex controllable shapes (see Figure 4) that include both large-scale buckling and small-scale wrinkling forms.

In one example [64], NIPA monomers with a BIS crosslinker in water and a catalyst, leads to the polymerization of a cross-linked elastic hydrogel, which undergoes a sharp, reversible, volume-reduction transition at a threshold temperature, allowing for temperature-controlled swelling in thin composite sheets. Another method [63] involves the photopatterning of polymer films to yield temperature-responsive gel sheets with the ability to print nearly continuous patterns of swelling. A third method [47] uses 3d printing of complex-fluid based inks to create bilayers with varying line density and anisotropy in order to achieve control over the extent and orientation of swelling. All these methods have been used to fabricate surfaces with constant Gaussian curvature (spherical caps, saddles, cones) or zero mean curvature (Enneper's surfaces), as well as more complex and nearly closed shapes. A natural question that these controlled experiments raise is the ability (or lack thereof) of the resulting patterns to approximate isometric immersions of prescribed metrics. From a mathematical perspective, this leads to questions of the asymptotic behavior of energy minimizing deformations and their associated energetics.

4.1. The setup.
In this and the next sections, we will consider a family $(\Omega^h, u^h, g, A, \mathcal{E}^h)_{h>0}$ (or more generally $(\Omega^h, u^h, g^h, A^h, \mathcal{E}^h)_{h>0}$) given in the function of the film's thickness parameter h. The main objective is now to predict the scaling of $\inf \mathcal{E}^h$ as $h \to 0$ and to analyze the asymptotic behavior of minimizing deformations u^h in relation to the curvatures associated with the prestrain A. We assume that $A = g^{1/2} : \overline{\Omega^1} \to \mathbb{R}^{3\times 3}_{\text{sym},>}$ is a smooth, symmetric, and positive definite tensor field on the unit thickness domain Ω^1, where for each $h > 0$ we define

$$\Omega^h = \omega \times \left(-\frac{h}{2}, \frac{h}{2}\right).$$

The open, bounded set $\omega \subset \mathbb{R}^2$ with Lipschitz boundary is viewed as the midplate of the thin film Ω^h, on which we pose the energy of elastic deformations,

$$(4.1) \qquad \mathcal{E}^h(u^h) = \frac{1}{h} \int_{\Omega^h} W\big((\nabla u^h)A^{-1}\big)\, \mathrm{d}x \qquad \text{for all } u^h \in W^{1,2}(\Omega^h, \mathbb{R}^3).$$

4.2. Isometric immersions and energy scaling.
As in section 3.2, there is a connection between $\inf \mathcal{E}^h$ and existence of isometric immersions, although this case is a bit more subtle. In the context of dimension reduction, this connection relies on the isometric immersions of the midplate metric $g(\cdot, 0)_{2\times 2}$ on ω into $\mathbb{R}^3$, namely parametrized surfaces $y : \omega \to \mathbb{R}^3$ with

$$(4.2) \qquad\qquad (\nabla y)^T \nabla y = g(\cdot, 0)_{2\times 2} \quad \text{in } \omega.$$

It turns out that existence of y with regularity $W^{2,2}$ is equivalent to the vanishing of $\inf \mathcal{E}^h$ of order square in the film's thickness $h \to 0$. The following result was proved first for $g = g(x')$ in [85] and then in the abstract setting of Riemannian manifolds in [71].

Theorem 4.1 ([12]). *Let $u^h \in W^{1,2}(\Omega^h, \mathbb{R}^3)$ satisfy $\mathcal{E}^h(u^h) \leq Ch^2$. Then we have:*

(i) Compactness. *There exist $c^h \in \mathbb{R}^3$ and $R^h \in SO(3)$ such that the rescaled deformations $y^h(x', x_3) = R^h u^h(x', hx_3) - c^h$ converge, up to a subsequence in $W^{1,2}(\Omega^1, \mathbb{R}^3)$, to some $y \in W^{2,2}(\Omega^1, \mathbb{R}^3)$ depending only on the tangential variable x' and satisfying (4.2).*
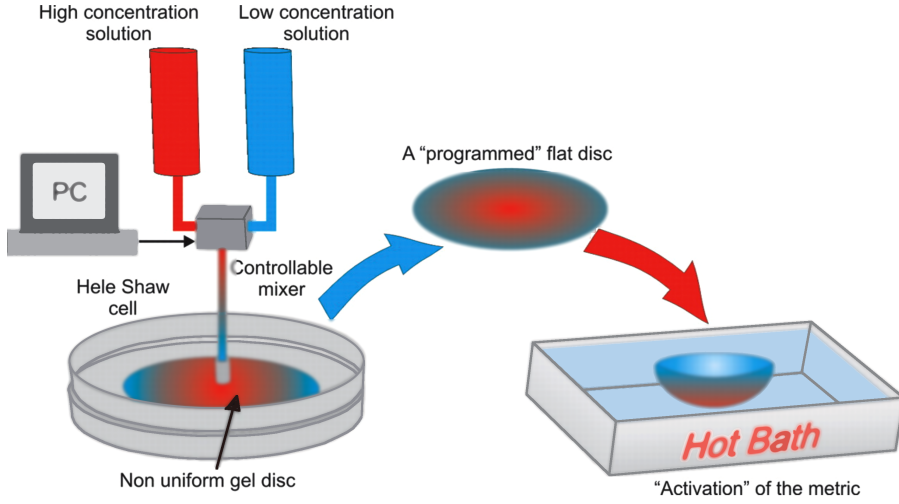
(a)
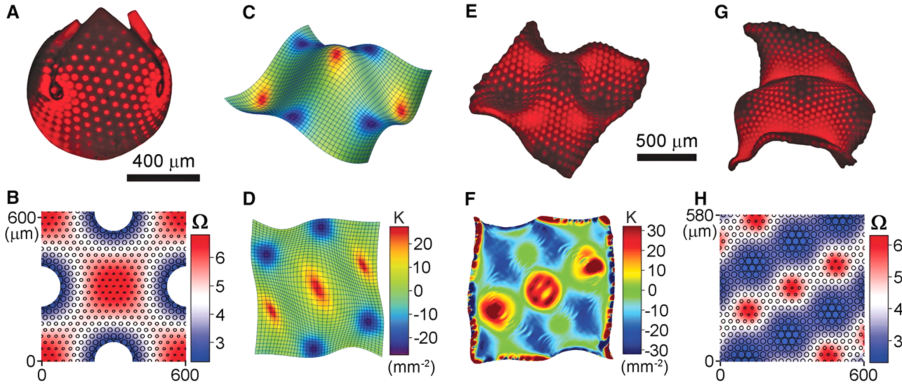
(b)

FIGURE 4. Imposing nontrivial target metrics in sheets of NIPA gels. The figures shown are (a) radially symmetric discs cast by injecting the solution into the gap between two flat glass plates through a central hole [64, ⓒ 2007, reprinted with permission from AAAS], (b) nonaxisymmetric swelling patterns constructed by half-tone gel lithography in [63, ⓒ 2012, reprinted with permission from AAAS].

(ii) *Liminf inequality.* *There holds the lower bound,*

$$(4.3) \quad \liminf_{h \to 0} \frac{1}{h^2} \mathcal{E}^h(u^h) \geq \mathcal{I}_{2,g}(y) = \frac{1}{24} \int_\omega \mathcal{Q}_2 \big(x', (\nabla y)^T \nabla \vec{b} - \frac{1}{2} \partial_3 g(\cdot, 0)_{2 \times 2} \big) \, \mathrm{d}x',$$

where $\mathcal{Q}_2(x', \cdot)$ are nonnegative quadratic forms given in terms of $D^2 W(\mathrm{Id}_3)$ (see (4.5)), and where $\vec{b}$ satisfies $[\partial_1 y, \partial_2 y, \vec{b}] \in SO(3)g(\cdot, 0)^{1/2}$. Equivalently, $\vec{b}$ is the Cosserat vector comprising the sheer, in addition to the direction $\vec{N}$

that is normal to the surface $y(\omega)$,

$$(4.4) \qquad \vec{b} = (\nabla y) g_{2\times2}^{-1} \begin{bmatrix} g_{13} \\ g_{23} \end{bmatrix} + \frac{\sqrt{\det g}}{\sqrt{\det g_{2\times2}}} \vec{N}, \quad with \ \ \vec{N} = \frac{\partial_1 y \times \partial_2 y}{|\partial_1 y \times \partial_2 y|}.$$

Moreover, there holds:

(iii) *Limsup inequality. For all $y \in W^{2,2}(\omega, \mathbb{R}^3)$ satisfying (4.2) there exists a sequence $\{u^h \in W^{1,2}(\Omega^h, \mathbb{R}^3)\}_{h\to0}$ for which convergence as in* (i) *above holds with $c_h = 0$, $R^h = \mathrm{Id}_3$, and*

$$\lim_{h\to0} \frac{1}{h^2} \mathcal{E}^h(u^h) = \mathcal{I}_{2,g}(y).$$

The energy density in (4.3) is given in terms of a family of quadratic forms $\mathcal{Q}_2(x', \cdot)$, that carry the two-dimensional reduction of the lowest-order nonzero term in the Taylor expansion of W close to its energy well $SO(3)$, namely,[4]

$$(4.5) \quad \mathcal{Q}_2(x', F_{2\times2}) = \min\big\{\mathcal{Q}_3\big(g(x',0)^{-1/2}\tilde{F}g(x',0)^{-1/2}\big),$$
$$\tilde{F} \in \mathbb{R}^{3\times3} \text{ with } \tilde{F}_{2\times2} = F_{2\times2}\big\},$$

where $\mathcal{Q}_3(F) = D^2W(\mathrm{Id}_3)(F, F)$.

From Theorem 4.1, one can deduce a counterpart of Proposition 3.1, stating an equivalent condition for existence of a $W^{2,2}$ isometric immersion of a two-dimensional metric in $\mathbb{R}^3$.

Corollary 4.2. *A smooth metric $\bar{g}$ on $\bar{\omega} \subset \mathbb{R}^2$ has an isometric immersion $y \in W^{2,2}(\omega, \mathbb{R}^3)$ if and only if $\inf \mathcal{E}^h \leq Ch^2$ for some (equivalently, for any) metric g on Ω^1 with $g(\cdot, 0)_{2\times2} = \bar{g}$.*

The question of existence of local isometric immersions of a given two-dimensional Riemannian manifold into $\mathbb{R}^3$ is a long-standing problem in differential geometry, its main feature consisting of finding the optimal regularity. By a classical result in [69], a $\mathcal{C}^1$ isometric embedding can be obtained by means of convex integration. This statement has been improved in [15] to $\mathcal{C}^{1,\alpha}$ regularity for all $\alpha < 1/7$ and analytic metrics $\bar{g}$, in [28] to $\mathcal{C}^2$ metrics, and in [32] for all $\alpha < 1/5$.[5] This regularity is far from $W^{2,2}$, where information about the second derivatives is also available. On the other hand, a smooth isometric immersion exists for some special cases, e.g., for smooth $\bar{g}$ with uniformly positive or negative Gaussian curvatures κ on bounded domains in $\mathbb{R}^2$ [52, Theorems 9.0.1 and 10.0.2]. Counterexamples to such theories are largely unexplored. By [58], there exists an analytic metric $\bar{g}$ with nonnegative κ on 2d sphere, with no local $\mathcal{C}^3$ isometric embedding. However, such metric always admits a $\mathcal{C}^{1,1}$ embedding [51, 55]; for a related example see also [102].

4.3. Γ-convergence and convergence of minimizers.
Statements (ii) and (iii) in Theorem 4.1 can be summarized in terms of Γ-*convergence* [30], which is one of the basic notions of convergence in the calculus of variations. A sequence of

---

[4]Both $\mathcal{Q}_3$ and all $\mathcal{Q}_2(x', \cdot)$ are nonnegative definite and depend only on the symmetric parts of their arguments, in view of assumptions on W.

[5]Of interest is also the result in [31], stating that for $\alpha > 1/2$ the Levi-Civita connection of any isometric immersion is induced by the Euclidean connection, whereas for any $\alpha < 1/2$ this property fails to hold.

functionals $\{F_n : Z \to \bar{\mathbb{R}}\}_{n\to\infty}$ defined on a metric space Z is said to Γ-converge to $F : Z \to \bar{\mathbb{R}}$ when the following two conditions hold:

(i) For any converging sequence $\{z_n\}_{n\to\infty}$ in Z we have

$$F\big(\lim_{n\to\infty} z_n\big) \leq \liminf_{n\to 0} F_n(z_n).$$

(ii) For every $z \in Z$ there exists $\{z_n\}_{n\to\infty}$ converging to z and such that $F(z) = \lim_{n\to\infty} F_n(z_n)$.

We then write $F_n \xrightarrow{\Gamma} F$. It is an exercise to show that if, additionally, there exists a compact set $K \subset Z$ with the property that $\inf_Z F_n = \inf_K F_n$ for all n, then we have the following:

- For any sequence $\{z_n \in K\}_{n\to\infty}$ of approximate minimizers to F_n, namely when $|F_n(z_n) - \inf_Z F_n| \to 0$, any accumulation point $z = \lim_{k\to\infty} z_{n_k}$ is a minimizer of F, i.e., $F(z) = \inf_X F$. In particular, F has at least one minimizer, and it has at least one minimizer in K.
- For every minimizer $z \in Z$ of F, there exists a *recovery sequence* of approximate minimizers $z_n \to z$ so that $|F_n(z_n) - \inf_Z F_n| \to 0$.

In view of the compactness assertion (i), Theorem 4.1 hence yields the following.

Corollary 4.3. *There holds, with respect to the strong convergence in $W^{1,2}(\Omega^1, \mathbb{R}^3)$,*

$$\frac{1}{h^2}\mathcal{E}^h\big(y(x', hx_3)\big) \xrightarrow{\Gamma} \begin{cases} \mathcal{I}_{2,g}(y) & \text{if } y \in W^{2,2}(\omega, \mathbb{R}^3) \text{ satisfies (4.2)}, \\ +\infty & \text{otherwise.} \end{cases}$$

Consequently, there is a one-to-one correspondence between limits of sequences of (global) approximate minimizers to the energies $\mathcal{E}^h$ and (global) minimizers of $\mathcal{I}_{2,g}$, provided that the induced metric $g(\cdot, 0)_{2\times 2}$ has a $W^{2,2}$ isometric immersion from ω to $\mathbb{R}^3$.

It is useful to make a couple of observations. First, we point out that, in general, one cannot expect $\mathcal{E}^h$ to posses a minimizer. The lower semicontinuity of the energy $\mathcal{E}$ in (3.1) allowing for the direct method of the calculus of variations, is tied to the quasiconvexity of the energy density, whereas $F \mapsto \text{dist}^2(F, SO(3))$ is not even rank-one convex [127, proof of Proposition 1.6].

Second, we comment on the relation of Corollary 4.3 with the experimental findings in [65] that constructed a thickness-parametrized family of axially symmetric hydrogel disks (see Figure 5). The explicit control on the radial concentration $c(r)$ of the temperature-responsive polymer (N-isopropylacrylamide) resulted in the ability to control the (locally isotropic) shrinkage factors of distances $\eta(r) = \eta(c(r))$ and led to the target metric $g_{2\times 2} = \text{d}r^2 + \kappa^{-1}\sin(\rho\kappa^{1/2})^2\text{d}\theta^2$ on the midplate $\omega = B(0, R)$, written in polar coordinates (r, θ) and in terms of the prescribed constant Gaussian curvature $\kappa \equiv \pm 0.0011$. While decreasing the thickness h, all disks with $\kappa > 0$ kept the same basic dome-like shape, with minor variations along the edge (see left column figures in Figure 5. The energy related to (4.1) was observed to stabilize as $h \to 0$, approaching a constant multiple of h^2 and exhibiting equipartition between bending and stretching. Hence, discs with positive curvature minimize their energy via the scenario in Corollary 4.3 by settling near the isometric immersion that is of the lowest bending content.

On the other hand, for $\kappa < 0$, the disks were observed to undergo a set of bifurcations in which the number of nodes (within a single wave configuration) increases and is roughly proportional to $h^{-1/2}$. Measuring the bending content in
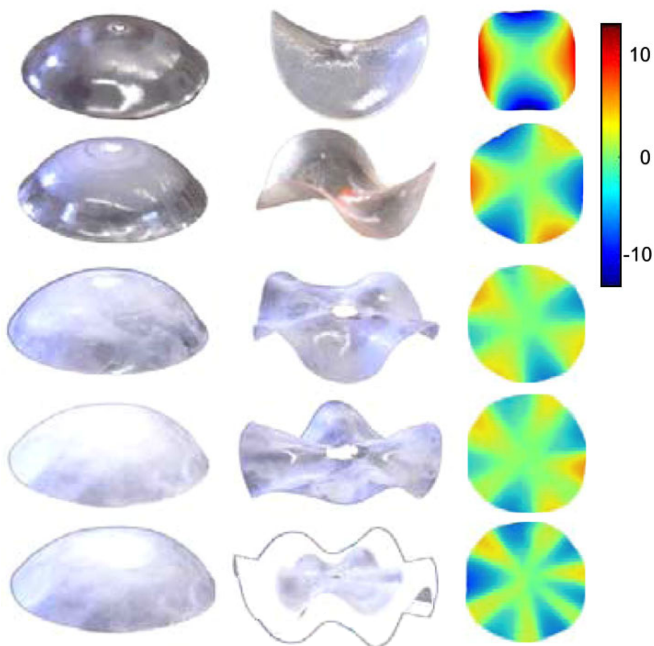
FIGURE 5. As a function of the thickness of a swollen sheet, one can achieve either elliptical or hyperbolic geometries. In the limit of vanishing thickness, the shape converges to the limit implied by the Γ-convergence result in Theorem 4.1 for the elliptic case (to a spherical dish) but shows an increasing preponderance to wrinkling on finer scales in the hyperbolic case. The multilobed swelling-induced wrinkling begs the question of the limiting behavior [65, © 2021, reprinted with permission of the American Physical Society].

this case led to $\mathcal{E}^h \sim h$ which seems to be linked to a stretching-driven process: the sharp increase of the bending content is compensated by a simultaneous decrease in the stretching content. Hence, hyperbolic disks minimize their energy via a set of bifurcations despite the existence of the smooth immersions y.

Open Problem 4.4. Analyze the possible origins of the diversity of behavior of the elliptic and hyperbolic disks in [65], as well as the discrepancy between the experimentally observed linear in h energy scaling and the quadratic scaling obtained in Corollary 4.3. The accuracy of the experiment determining the target metric g is finite, and the sensitivity to perturbations seems to be more pronounced in the negative Gauss curvature regimes.

4.4. **Energy scaling from convex integration.** A separate energy bound may be obtained by constructing deformations u^h through the Kirchhoff–Love extension of isometric immersions of regularity $\mathcal{C}^{1,\alpha}$. Existence of such is guaranteed by techniques of convex integration [32] for all $\alpha < 1/5$, and this threshold implies the particular energy scaling bound in Proposition 4.5 below. If we could take

$\alpha < 1/3$ (corresponding to the so-called "one step" in each "stage" of the Nash–Kuiper iteration scheme), then the exponent would be $\beta < 1$. If we could take $\alpha < 1/2$ for the flexibility threshold as conjectured in [33], then $\beta < 4/3$. Recall that existence of a $W^{2,2}$ isometric immersion implies that $\inf \mathcal{E}^h$ may be further decreased to Ch^2.

Proposition 4.5. *Assume that $\omega \subset \mathbb{R}^2$ is simply connected with $\mathcal{C}^{1,1}$-regular boundary. Then*

$$\inf \mathcal{E}^h \leq Ch^\beta \qquad for\ all\ \ \beta < \frac{2}{3}.$$

Proof. Fix $\alpha \in (0, 1/5)$ and let $y \in \mathcal{C}^{1,\alpha}(\bar{\omega}, \mathbb{R}^3)$ satisfy (4.2). Define the vector field $\vec{b}_1 \in \mathcal{C}^{0,\alpha}(\bar{\omega}, \mathbb{R}^3)$ by (4.4), yielding the auxiliary matrix field,

$$B = \begin{bmatrix} \partial_1 y, & \partial_2 y, & \vec{b} \end{bmatrix} \in \mathcal{C}^{0,\alpha}(\bar{\omega}, \mathbb{R}^{3\times3}) \quad \text{satisfying } \det B > 0, \ \ B^T B = g(\cdot, 0) \ \text{ in } \bar{\omega}.$$

The last assertion above implies that

(4.6) $$B(x')A(x', 0)^{-1} \in SO(3) \quad \text{ for all } x' \in \bar{\omega}.$$

Regularize now $y, \vec{b}$ to $y_\varepsilon, b_\varepsilon \in \mathcal{C}^\infty(\bar{\omega}, \mathbb{R}^3)$ by means of the family of standard convolution kernels $\{\phi_\varepsilon(x) = \varepsilon^{-2}\phi(x/\varepsilon)\}_{\varepsilon \to 0}$, where ε is a power of h to be chosen later:

$$y_\varepsilon = y * \phi_\varepsilon, \quad b_\varepsilon = \vec{b} * \phi_\varepsilon, \quad B_\varepsilon = B * \phi_\varepsilon, \quad \text{and} \quad \varepsilon = h^t.$$

We will utilize the following bound, resulting from the commutator estimate [28, Lemma 1],

(4.7)
$$\begin{aligned}
\left\| B_\varepsilon^T B_\varepsilon - g(\cdot, 0) \right\|_{\mathcal{C}^0(\omega)} &\leq \left\| B_\varepsilon^T B_\varepsilon - (B^T B) * \phi_\varepsilon \right\|_{\mathcal{C}^0(\omega)} \\
&\quad + \left\| g(\cdot, 0) * \phi_\varepsilon - g(\cdot, 0) \right\|_{\mathcal{C}^0(\omega)} \\
&\leq C\varepsilon^{2\alpha} + C\varepsilon^2 \leq C\varepsilon^{2\alpha},
\end{aligned}$$

where the $C\varepsilon^2$ bound results by Taylor-expanding g up to second-order terms. Denoting $D_\varepsilon = \begin{bmatrix} \partial_1 b_\varepsilon, & \partial_2 b_\varepsilon, & 0 \end{bmatrix}$, we get the uniform bounds,

(4.8) $$\|B_\varepsilon - B\|_{\mathcal{C}^0(\omega)} \leq C\varepsilon^\alpha, \qquad \|D_\varepsilon\|_{\mathcal{C}^0(\omega)} \leq C\varepsilon^{\alpha-1}.$$

Consider the sequence of deformations $u^h \in \mathcal{C}^\infty(\bar{\Omega}^h, \mathbb{R}^3)$ in

$$u^h(x', x_3) = y_\varepsilon(x') + x_3 b_\varepsilon(x'), \quad \text{so that } \nabla u^h = B_\varepsilon + x_3 D_\varepsilon.$$

In particular, $\|\nabla u^h(x', hx_3) - B(x')\|_{\mathcal{C}^0(\Omega^1)} \leq C(\varepsilon^\alpha + h\varepsilon^{\alpha-1})$ and since $A(x', hx_3)^{-1} = A(x')^{-1} + \mathcal{O}(h)$ for all $(x', x_3) \in \Omega^1$, it follows by (4.6) that

$$\begin{aligned}
\left\| \text{dist}\left(\nabla u^h A^{-1}, SO(3)\right) \right\|_{\mathcal{C}^0(\Omega^h)} &\leq \left\| \nabla u^h A^{-1}(x', hx_3) - BA^{-1}(x', 0) \right\|_{\mathcal{C}^0(\Omega^1)} \\
&\leq C(\varepsilon^\alpha + h\varepsilon^{\alpha-1} + h) \to 0 \quad \text{as } h \to 0,
\end{aligned}$$

if only $h\varepsilon^{\alpha-1} \to 0$. We then use the polar decomposition theorem and conclude that for some $R^h = R^h(x', hx_3) \in SO(3)$ there holds

$$\begin{aligned}
R^h \nabla u^h(x', hx_3)A(x', hx_3)^{-1} &= \left(A^{-1}(\nabla u^h)^T \nabla u^h A^{-1}\right)^{1/2}(x', hx_3) \\
&= \left(A(x', hx_3)^{-1}(B_\varepsilon^T B_\varepsilon(x') + \mathcal{O}(hD_\varepsilon))A(x', hx_3)^{-1}\right)^{1/2} \\
&= \left((A(x', 0)^{-1} + \mathcal{O}(h))(g(x', 0) + \mathcal{O}(\varepsilon^{2\alpha} + h\varepsilon^{\alpha-1})(A(x', 0)^{-1} + \mathcal{O}(h))\right)^{1/2} \\
&= \left(\text{Id}_3 + \mathcal{O}(h + \varepsilon^{2\alpha} + h\varepsilon^{\alpha-1})\right)^{1/2} = \text{Id}_3 + \mathcal{O}(h + \varepsilon^{2\alpha} + h\varepsilon^{\alpha-1}),
\end{aligned}$$

by virtue of (4.7) and (4.8). Consequently, we obtain the energy bound

$$\mathcal{E}^h(u^h) = \int_{\Omega^1} W\big(R^h \nabla u^h (A^h)^{-1}(x', hx_3)\big) \, \mathrm{d}(x', x_3)$$

$$\leq C\big(h + \varepsilon^{2\alpha} + h\varepsilon^{\alpha-1}\big)^2 = C\big(h + h^{2\alpha t} + h^{1+(\alpha-1)t}\big)^2.$$

Minimizing the right-hand side above corresponds to maximizing the minimal of the three displayed exponents. We hence choose t in $\varepsilon = h^t$ so that $2\alpha t = 1 + (\alpha - 1)t$, namely $t = \frac{1}{\alpha+1}$. This leads to the estimate,

$$\inf \mathcal{E}^h \leq C h^{\frac{4\alpha}{\alpha+1}} \quad \text{for all } \alpha < \frac{1}{5},$$

which completes the proof.   □

Open Problem 4.6. Analyze the limiting behavior of minimizing deformations in the intermediate energy scaling regime $\inf \mathcal{E}^h \simeq Ch^\beta$ for $\beta \in [2/3, 2)$. Is it necessarily guided by an isometric immersion of some prescribed regularity? Find the Γ-limits of scaled energies $\frac{1}{h^\beta} \mathcal{E}^h$.

4.5. **The intermediate scalings.** As a point of comparison, we remark that higher energy scalings $\inf \mathcal{E}^h \sim h^\beta$ may result due to the sheet being forced at a boundary, due to the presence of external forces associated with gravity, the presence of an elastic substrate, etc., all of which can lead to a range of microstructural patterns that are wrinkle-like. From Theorem 4.1, we recall that the regime $\beta \geq 2$ pertains to the "no wrinkling" family of almost minimizing deformations, that are perturbations of a $W^{2,2}$ isometric immersion. While the systematic description of the singular limits associated with exponents $\beta < 2$ is not yet available, there are a number of examples of the variety of emerging patterns that are illustrative.

When a thin film is either clamped or weakly adhered to a substrate and subject to thermal or mechanical loads, it can buckle and blister [5, 9, 10, 61]; in these cases, the energy scaling estimates yield $\beta = 1$. A similar exponent is also seen in cases when a thin film wrinkles in response to metric constraints [5], or forms a hanging drape exhibiting fluted patterns that coarsen as a function of distance from the point of support [6, 22]. In related experiments and theory, when a thin shell of nonzero curvature is placed on a liquid bath, it forms complex wrinkling patterns [117] with a range of β between 0 and 1, depending on the strengths of the elastic and substrate forces. Moving from sheets or surfaces toward ribbons that have all three dimensions far from each other, papers [67, 68] analyze wrinkling in the center of a stretched and twisted ribbon and find that $\beta = 4/3$. Moving away from situations associated with nonlocal wrinkled microstructures, there have been a number of studies of localized structures associated with the theoretical and experimental analysis of *conical singularities* that arise in crumpled sheets [19–21] that have been recently analyzed mathematically [94, 100, 101] and lead to energetic estimates for this singularity of the form $\mathcal{E}^h \sim h^2 \log(1/h)$. And, in cases where the sheet is strongly creased, as in *origami patterns*, energy levels are associated with $\beta = 5/3$ [29, 121]. We remark that the mentioned papers do not address the dimension reduction but rather analyze the chosen actual configuration of the prestrained sheet.

Closely related is also the literature on shape selection in non-Euclidean plates, exhibiting hierarchical *buckling patterns* in the limit of zero strain plates with $\beta = 2$, where the complex morphology is due to nonsmooth energy minimization [44–46].

Various geometrically nonlinear thin plate theories have been used to analyze the self-similar structures with metric asymptotically flat at infinity [4] that include a disk with edge-localized growth [40], the shape of a long leaf [89], or torn plastic sheets [107].

5. HIERARCHY OF LIMITING THEORIES IN THE NONWRINKLING REGIMES

We now detail the complete set of results relating the context of dimension reduction in non-Euclidean elasticity with the quantitative immersability of Riemann metrics. As shown in Figure 6, a range of distinct behaviors of a thin sheet takes place in response to the prestrains of different orders. Within the formalism of finite elasticity, such patterns result from the sheet buckling to relieve growth or swelling induced by the residual strains. These will be measured via the scaling of the prestrain metric's Riemann curvatures, as explained below.

(a)   (b)

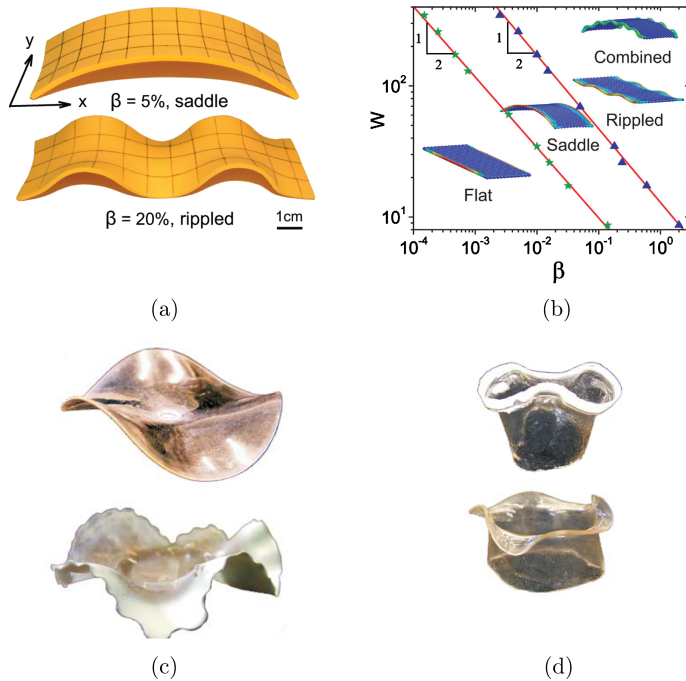(c)   (d)

FIGURE 6. A range of patterns arise when a thin sheet is inhomogeneously stretched plastically or swells in response to a solvent. (a) By dragging one's nails along the edges of a foam strip weakly, a flat surface transitions to one that is hyperbolic. (b) The same process carried out strongly leads to a surface that is strongly rippled, much like the edges of a leaf [89]. (c) Thin sheets of a circular gel disk deform into a hyperbolic surface with two lobes. (d) Thinner sheets deform into multilobed sheets which are able to relieve the swelling-induced frustration by changing their curvature on multiple scales [64, © 2012, reprinted with permission from AAAS].

5.1. **The energy scaling quantization.** Observe that in view of Theorem 4.1, there holds $\lim_{h\to 0} \frac{1}{h^2} \inf \mathcal{E}^h = 0$ if and only if there exists $y \in W^{2,2}(\omega, \mathbb{R}^3)$ such that with $\vec{b}$ as in (4.4),

$$(5.1) \quad (\nabla y)^T \nabla y = g(\cdot, 0)_{2\times 2} \quad \text{and} \quad \text{sym}\left((\nabla y)^T \nabla \vec{b}\right) = \frac{1}{2}\partial_3 g(\cdot, 0)_{2\times 2} \quad \text{in } \omega.$$

The above compatibility of tensors $g(\cdot, 0)_{2\times 2}$ and $\partial_3 g(\cdot, 0)_{2\times 2}$ is equivalent to the satisfaction of the Gauss–Codazzi–Meinardi equations for the related first and second fundamental forms

$$I = (\nabla y)^T \nabla y,$$

$$II = (\nabla y)^T \nabla \vec{N} = \sqrt{g^{33}}\left(\text{sym}((\nabla y)^T \nabla \vec{b}) - \frac{1}{2}\partial_3 g(\cdot, 0)_{2\times 2}\right) - \frac{1}{\sqrt{g^{33}}}\left[\Gamma_{ij}^3(\cdot, 0)\right]_{i,j=1\cdots 2}.$$

These three compatibility conditions turn out to be precisely expressed by

$$(5.2) \qquad \mathcal{R}_{12,12}(\cdot, 0) = \mathcal{R}_{12,13}(\cdot, 0) = \mathcal{R}_{12,23}(\cdot, 0) = 0 \quad \text{in } \omega.$$

Corollary 5.1 ([12, 76, 88]). *Condition $\frac{1}{h^2}\inf \mathcal{E}^h \to 0$ as $h \to 0$ is equivalent to $\min \mathcal{I}_{2,g} = 0$, and further to (5.2). In case (5.2) holds, we have $\text{Ker }\mathcal{I}_{2,g} = \{Ry_0 + c; \ R \in SO(3), \ c \in \mathbb{R}^3\}$, where $y_0 : \bar{\omega} \to \mathbb{R}^3$ is a unique "compatible" smooth isometric immersion of $g(\cdot, 0)_{2\times 2}$ satisfying (5.1) together with its corresponding Cosserat vector $\vec{b} = \vec{b}_1$. Moreover, $\inf \mathcal{E}^h \leq Ch^4$.*

To justify the last assertion, we define the family $\{u^h\}_{h\to 0}$ as in the proof of Proposition 4.5,

$$u^h(x', x_3) = y_0(x') + x_3 \vec{b}_1(x') + \frac{x_3^2}{2}\vec{b}(x'), \quad \text{so that} \quad \nabla u^h = B_0 + x_3 B_1 + \mathcal{O}(x_3^2).$$

By polar decomposition, the tensor $(\nabla u^h)A^{-1}$ coincides with

$$Z \doteq \left(\left((\nabla u^h)A^{-1}\right)^T\left((\nabla u^h)A^{-1}\right)\right)^{1/2}$$

up to a rotation. Since

$$(\nabla u^h)^T \nabla u^h = B_0^T B_0 + 2x_3 \text{sym}(B_0^T B_1) + \mathcal{O}(x_3^2),$$
$$A(x', x_3)^{-1} = A(x', 0)^{-1} - x_3 A^{-1}(\partial_3 A)A^{-1}(x', 0) + \mathcal{O}(x_3^2),$$

it follows that Z^2 equals

$$A^{-1}(\nabla u^h)^T(\nabla u^h)A^{-1} = A^{-1}\left(g(x', 0) + 2x_3 \text{sym}(B_0^T B_1) + \mathcal{O}(x_3^2)\right)A^{-1}$$
$$= \text{Id}_3 + 2x_3 A^{-1}\text{sym}\left(B_0^T B_1 - A\partial_3 A\right)A^{-1}(x', 0) + \mathcal{O}(x_3^2)$$
$$= \text{Id}_3 + \mathcal{O}(x_3^2).$$

The last equality above is achieved by choosing $\vec{b}_2 : \bar{\omega} \to \mathbb{R}^3$ such that

$$\text{sym}\left(B_0^T B_1 - A\partial_3 A(\cdot, 0)\right) = 0,$$

because the 2×2 minor of the indicated tensor is zero due to (5.1). Consequently,

$$\mathcal{E}^h(u^h) = \frac{1}{h}\int_{\Omega^h} W(Z) \leq \frac{1}{h}\int_{\Omega^h} W\left(\text{Id}_3 + \mathcal{O}(x_3^2)\right) \leq Ch^4.$$

The following general result proves that the only viable scalings of $\inf \mathcal{E}^h \sim h^\beta$ in the regime $\beta \geq 2$ are the even powers $\beta = 2n$.

Theorem 5.2 ([75]). *For every $n \geq 2$, if $\lim_{h \to 0} \frac{1}{h^{2n}} \inf \mathcal{E}^h = 0$, then $\inf \mathcal{E}^h \leq Ch^{2(n+1)}$. Further, the following three statements are equivalent:*

(i) $\inf \mathcal{E}^h \leq Ch^{2(n+1)}$.

(ii) $\mathcal{R}_{12,12}(\cdot, 0) = \mathcal{R}_{12,13}(\cdot, 0) = \mathcal{R}_{12,23}(\cdot, 0) = 0$ *and* $\partial_3^{(k)} \mathcal{R}_{i3,j3}(\cdot, 0) = 0$ *in* ω, *for all* $k = 0 \cdots n - 2$ *and all* $i, j = 1 \cdots 2$.

(iii) *There exist smooth fields* $y_0, \{\vec{b}_k\}_{k=1}^{n+1} : \bar{\omega} \to \mathbb{R}^3$ *and frames*

$$\left\{ B_k = \left[\partial_1 \vec{b}_k, \ \partial_2 \vec{b}_k, \ \vec{b}_{k+1} \right] \right\}_{k=1}^n,$$
$$B_0 = \left[\partial_1 y_0, \ \partial_2 y_0, \ \vec{b}_1 \right],$$

such that $\sum_{k=0}^m \binom{m}{k} B_k^T B_{m-k} - \partial_3^{(m)} g(\cdot, 0) = 0$ *for all* $m = 0 \cdots n$. *Equivalently,* $\left(\sum_{k=0}^n \frac{x_3^k}{k!} B_k \right)^T \left(\sum_{k=0}^n \frac{x_3^k}{k!} B_k \right) = g(x', x_3) + \mathcal{O}(h^{n+1})$ *on* Ω^h *as* $h \to 0$. *The field* y_0 *is the unique smooth isometric immersion of* $g(\cdot, 0)_{2 \times 2}$ *into* $\mathbb{R}^3$ *for which* $\mathcal{I}_{2,g}(y_0) = 0$.

We note that if $\mathcal{R}(\cdot, 0) = 0$ and $\partial_3^{(m)} \left[\mathcal{R}_{i3,j3}(\cdot, 0) \right]_{i,j=1\cdots2} = 0$ on ω for all $m = 0 \cdots n - 2$ but $\partial_3^{(n-1)} \left[\mathcal{R}_{i3,j3}(\cdot, 0) \right]_{i,j=1\cdots2} \neq 0$, then $ch^{2(n+1)} \leq \inf \mathcal{E}^h \leq Ch^{2(n+1)}$ for some $c, C > 0$. The conformal metrics $g(x', x_3) = e^{2\phi(x_3)} \mathrm{Id}_3$ provide a class of examples for the viability of all scalings $\inf \mathcal{E}^h \sim h^{2n}$ by choosing $\phi^{(k)}(0) = 0$ for $k = 1 \cdots n - 1$ and $\phi^{(n)}(0) \neq 0$.

5.2. The infinite hierarchy of Γ-limits.

To derive the counterpart of Corollary 4.3 for higher energy scalings, one observes the following compactness properties under the assumption that $\mathcal{E}^h(u^h) \leq Ch^{2(n+1)}$, for some $n \geq 1$. First ([75]), there exist $c^h \in \mathbb{R}^3$, $R^h \in SO(3)$ such that

$$V^h(x') = \frac{1}{h^n} \int_{-h/2}^{h/2} (\bar{R}^h)^T \left(u^h(x', x_3) - c^h \right) - \left(y_0(x') + \sum_{k=1}^n \frac{x_3^k}{k!} \vec{b}_k(x') \right) \, \mathrm{d}x_3$$

converge as $h \to 0$ in $W^{1,2}(\omega, \mathbb{R}^3)$, to a limiting displacement V that is an infinitesimal isometry

$$V \in \mathcal{V}_{y_0} = \left\{ V \in W^{2,2}(\omega, \mathbb{R}^3); \ \mathrm{sym}\left((\nabla y_0)^T \nabla V \right) = 0 \right\}.$$

In particular, there exists $\vec{p} \in W^{1,2}(\omega, \mathbb{R}^3)$ with $\mathrm{sym}\left(B_0^T [\nabla V, \ \vec{p}] \right) = 0$. Second, the strains

$$\frac{1}{h} \mathrm{sym}\left((\nabla y_0)^T \nabla V^h \right)$$

converge as $h \to 0$, weakly in $L^2(\omega, \mathbb{R}^{2 \times 2})$ to a limiting $\mathbb{S}$ in the finite strain space

$$\mathbb{S} \in \mathcal{S}_{y_0} = \mathrm{cl}_{L^2} \left\{ \mathrm{sym}((\nabla y_0)^T \nabla w_n); \ w_n \in W^{1,2}(\omega, \mathbb{R}^3) \right\}.$$

The space $\mathcal{S}_{y_0}$ can be identified, in particular, in the following two cases on ω simply connected. When $y_0 = \mathrm{id}_2$, then $\mathcal{S}_{y_0} = \{ \mathbb{S} \in L^2(\omega, \mathbb{R}^{2 \times 2}_{\mathrm{sym}}); \ \mathrm{curl \ curl} \ \mathbb{S} = 0 \}$. When the Gauss curvature $\kappa((\nabla y_0)^T \nabla y_0) = \kappa(g(\cdot, 0)_{2 \times 2}) > 0$ on $\bar{\omega}$, then $\mathcal{S}_{y_0} = L^2(\omega, \mathbb{R}^{2 \times 2}_{\mathrm{sym}})$, as shown in [82].

Further, we have the following Γ-convergence results with respect to the above compactness statements. The infinite hierarchy of the limiting prestrained theories is gathered in Table 1.

TABLE 1. The infinite hierarchy of Γ-limits for prestrained films, scaling $\beta \geq 2$

β	asymptotic expansion	constraint / regularity	limiting energy $\mathcal{I}_{\beta,g}$
2	$y(x')$ $\{3d:\ y(x') + x_3 \vec{b}(x')\}$	$y \in W^{2,2}$ $(\nabla y)^T \nabla y = g(x',0)_{2\times 2}$	$c\|(\nabla y)^T \vec{b} - \frac{1}{2}\partial_3 g(x',0)_{2\times 2}\|_{\mathbb{Q}_2}^2$ $[\partial_3 y, \partial_2 y, \vec{b}] \in SO(3)g(x',0)^{1/2}$
4	$y_0(x') + hV(x')$ $\quad + h^2 w^h(x')$	$\mathcal{R}_{12,12}, \mathcal{R}_{12,13}, \mathcal{R}_{12,23}(x',0) = 0$ $((\nabla y_0)^T \nabla V)_{\mathrm{sym}} = 0,$ $((\nabla y_0)^T \nabla w^h)_{\mathrm{sym}} \to \mathbb{S}$ $V \in W^{2,2}(\omega, \mathbb{R}),\ w^h \in W^{1,2}(\omega, \mathbb{R}^3)$	$c_1 \|\frac{1}{2}(\nabla V)^T \nabla V + \mathbb{S} + \frac{1}{24}(\nabla \vec{b}_1)^T \nabla \vec{b}_1$ $\quad - \frac{1}{48}\partial_{33}g(x',0)_{2\times 2}\|_{\mathbb{Q}_2}^2$ $\quad + c_2 \|(\nabla y_0)^T \nabla \vec{p} + (\nabla V)^T \nabla \vec{b}_1\|_{\mathbb{Q}_2}^2$ $\quad + c_3 \|[\mathcal{R}_{i3,j3}(x',0)]_{i,j=1,2}\|_{\mathbb{Q}_2}^2$
6 $\vdots$	$y_0(x') + h^2 V(x')$	$\mathcal{R}_{ab,cd}(x',0) = 0$ $((\nabla y_0)^T \nabla V)_{\mathrm{sym}} = 0,\ V \in W^{2,2}$	$c_2 \|(\nabla y_0)^T \nabla \vec{p} + (\nabla V)^T \nabla \vec{b}_1 + \alpha[\partial_3 \mathcal{R}]\|_{\mathbb{Q}_2}^2$ $+ c_3 \|\mathbb{P}_{\mathcal{S}_{y_0}^\perp}[\partial_3 \mathcal{R}]\|_{\mathbb{Q}_2}^2 + c_4 \|\mathbb{P}_{\mathcal{S}_{y_0}}[\partial_3 \mathcal{R}]\|_{\mathbb{Q}_2}^2$
$2n$ $\vdots$	$y_0(x') + h^{n-1}V(x')$ $\{3d: y_0 + \sum_{k=1}^{n-1} \frac{x_3^k}{k!}\vec{b}_k(x')$ $\quad + h^{n-1}V(x')$ $\quad + h^{n-1}x_3\vec{p}(x')\}$	$\mathcal{R}_{ab,cd}(x',0) = 0$ $[\partial_3^{(k)}\mathcal{R}](x',0) = 0\ \forall k \leq n-3$ $((\nabla y_0)^T \nabla V)_{\mathrm{sym}} = 0,\ V \in W^{2,2}$	$c_2 \|(\nabla y_0)^T \nabla \vec{p} + (\nabla V)^T \nabla \vec{b}_1 + \alpha[\partial_3^{(n-2)}\mathcal{R}]\|_{\mathbb{Q}_2}^2$ $+ c_3 \|\mathbb{P}_{\mathcal{S}_{y_0}^\perp}[\partial_3^{(n-2)}\mathcal{R}]\|_{\mathbb{Q}_2}^2$ $+ c_4 \|\mathbb{P}_{\mathcal{S}_{y_0}}[\partial_3^{(n-2)}R]\|_{\mathbb{Q}_2}^2$

Theorem 5.3 ([75, 76]). *In the energy* (4.1) *scaling regimes indicated in Theorem 5.2, the following holds. For the von Kármán-like regime, we have for all $V \in \mathcal{V}_{y_0}$ and $\mathbb{S} \in \mathcal{S}_{y_0}$ that*

$$\frac{1}{h^4}\mathcal{E}^h \xrightarrow{\Gamma} \mathcal{I}_{4,g}(V,\mathbb{S})$$
$$= \frac{1}{2}\int_\omega \mathcal{Q}_2\Big(x', \underbrace{\mathbb{S}(x') + \frac{1}{2}\nabla V(x')^T \nabla V(x') + \frac{1}{24}\nabla \vec{b}_1(x')^T \nabla \vec{b}_1(x') - \frac{1}{48}\partial_{33}g(x',0)_{2\times 2}}_{stretching}\Big)\ \mathrm{d}x'$$
$$+ \frac{1}{24}\int_\omega \mathcal{Q}_2\Big(x', \underbrace{\nabla y_0(x')^T \nabla \vec{p}(x') + \nabla V(x')^T \nabla \vec{b}_1(x')}_{bending}\Big)\ \mathrm{d}x'$$
$$+ \frac{1}{1440}\int_\omega \mathcal{Q}_2\Big(x', \underbrace{\begin{bmatrix} \mathcal{R}_{13,13} & \mathcal{R}_{13,23} \\ \mathcal{R}_{13,23} & \mathcal{R}_{23,23} \end{bmatrix}}_{curvature}\Big)\ \mathrm{d}x'.$$

For all $n \geq 1$ (which is the case parallel to linear elasticity), we have for all $V \in \mathcal{V}_{y_0}$ that

$$\frac{1}{h^{2(n+1)}}\mathcal{E}^h \xrightarrow{\Gamma} \mathcal{I}_{2(n+1),g}(V)$$
$$= \frac{1}{24}\int_\omega \mathcal{Q}_2\Big(x', \underbrace{(\nabla y_0)^T \nabla \vec{p} + (\nabla V)^T \nabla \vec{b}_1 + \alpha_n\big[\partial_3^{(n-1)}\mathcal{R}_{i3,j3}\big]_{i,j=1\cdots 2}}_{bending}\Big)\ \mathrm{d}x'$$
$$+ \beta_n \int_\omega \mathcal{Q}_2\Big(x', \mathbb{P}_{\mathcal{S}_{y_0}^\perp}\big(\big[\partial_3^{(n-1)}\mathcal{R}_{i3,j3}\big]_{i,j=1\cdots 2}\big)\Big)\ \mathrm{d}x'$$
$$+ \gamma_n \int_\omega \mathcal{Q}_2\Big(x', \mathbb{P}_{\mathcal{S}_{y_0}}\big(\big[\partial_3^{(n-1)}\mathcal{R}_{i3,j3}\big]_{i,j=1\cdots 2}\big)\Big)\ \mathrm{d}x',$$

where $\mathbb{P}_{\mathcal{S}_{y_0}}, \mathbb{P}_{\mathcal{S}_{y_0}^\perp}$ denote orthogonal projections onto $\mathcal{S}_{y_0}$ and onto its L^2-orthogonal complement $\mathcal{S}_{y_0}^\perp$. The coefficients $\alpha_n, \beta_n, \gamma_n \geq 0$ are given explicitly, and $\alpha_n \neq 0$ if and only if n is even.

The functional $\mathcal{I}_{4,g}$ is indeed a von Kármán-like energy, consisting of stretching and bending (with respect to the unique, up-to-rigid motions, smooth isometric

immersion y_0 that has zero energy in the prior Γ-limit (4.3)) plus a new term quantifying the remaining three Riemann curvatures. When $g = \mathrm{Id}_3$, then $\mathcal{I}_{4,g}(V, \mathbb{S})$ reduces to the classical von Kármán functional, given in terms of the out-of-plane displacement v in $V = (\alpha x^\perp + \beta, v)$ for which $\vec{p} = (-\nabla v, 0)$, and the in-plane displacement w in $\mathbb{S} = \mathrm{sym}\,\nabla w$,

$$(5.3) \qquad \mathcal{I}_4(v, w) = \frac{1}{2} \int_\omega \mathcal{Q}_2\big(\mathrm{sym}\,\nabla w + \frac{1}{2}\nabla v \otimes \nabla v\big)\,\mathrm{d}x' + \frac{1}{24} \int_\omega \mathcal{Q}_2(\nabla^2 v)\,\mathrm{d}x'.$$

We point out in passing that in [35, 36], a variant of the Föppl–von Kármán equilibrium equations has been formally derived from finite incompressible elasticity via the multiplicative decomposition of deformation gradient [104] used in finite plasticity [73] and hyperelastic growth.

Likewise, each $\mathcal{I}_{2(n+1),\mathrm{Id}_3}$ reduces to the classical linear elasticity,

$$(5.4) \qquad\qquad\qquad \mathcal{I}_{2(n+1)}(v) = \frac{1}{24} \int_\omega \mathcal{Q}_2\big(\nabla^2 v\big)\,\mathrm{d}x'.$$

In the present geometric context, the bending term $(\nabla y_0)^T \nabla\vec{p} + (\nabla V)^T \nabla\vec{b}_1$ in $\mathcal{I}_{2(n+1),g}$ is of order $h^n x_3$ and it interacts with the curvature

$$\big[\partial_3^{(n-1)}\mathcal{R}_{i3,j3}(\cdot, 0)\big]_{i,j=1\cdots 2},$$

which is of order x_3^{n+1}. The interaction occurs only when the two terms have the same parity in x_3, namely at even n, so that $\alpha_n = 0$ for all n odd. The two remaining terms measure the L^2 norm of $\big[\partial_3^{(n-1)}R_{i3,j3}(\cdot, 0)\big]_{i,j=1\cdots 2}$, with distinct weights assigned to $\mathcal{S}_{y_0}$ and $(\mathcal{S}_{y_0})^\perp$ projections, again according to the parity of n. We also have $\inf_{V_{y_0}}\mathcal{I}_{2(n+1),g} \sim \big\|\big[\partial_3^{(n-1)}\mathcal{R}_{i3,j3}(\cdot, 0)\big]_{i,j=1\cdots 2}\big\|_{L^2(\omega)}^2$.

Remark 5.4. Parallel general results can be derived in the abstract setting of Riemannian manifolds: in [70, 71] Γ-convergence statements were proved for any dimension ambient manifold and codimension midplate, in the scaling regimes $\mathcal{O}(h^2)$ and $\mathcal{O}(1)$, respectively. In [92], the authors analyze scaling orders $o(h^2)$, $\mathcal{O}(h^4)$, and $o(h^4)$.

6. Floral morphogenesis, weak prestrain, and special solutions of Monge–Ampère equations

We digress in this section to consider an interesting set of questions inspired by the remarkable examples of floral morphogenesis resembling parts of a pseudo-sphere (see Figure 7) altered by the presence of ripples along the free boundary. Early work [99], revisited in [98], suggested that information on the profile of the boundary of a plant's leaf fluctuating in a direction transversal to the leaf's surface can be read from the Jacobian of the conformal mapping corresponding to an isometric embedding of the given prestrain metric. This leads to the question of constructing solutions to the classical Monge–Ampère equation, without prescribed boundary conditions but approximating the smallest bending content possible while preserving the regularity that allows for the consistent association of this bending content.

A similar point of view has been adopted in [44] for the choice of the target midplate metric, $g_{2\times 2} = \mathrm{Id}_2 + 2\varepsilon^2 f(x_2)\mathrm{d}x_1^2$, posed on the infinite strip $\omega = \mathbb{R} \times [0, W]$. The coefficient field $f(x_2)$ corresponds to the x_2-dependent growth in the
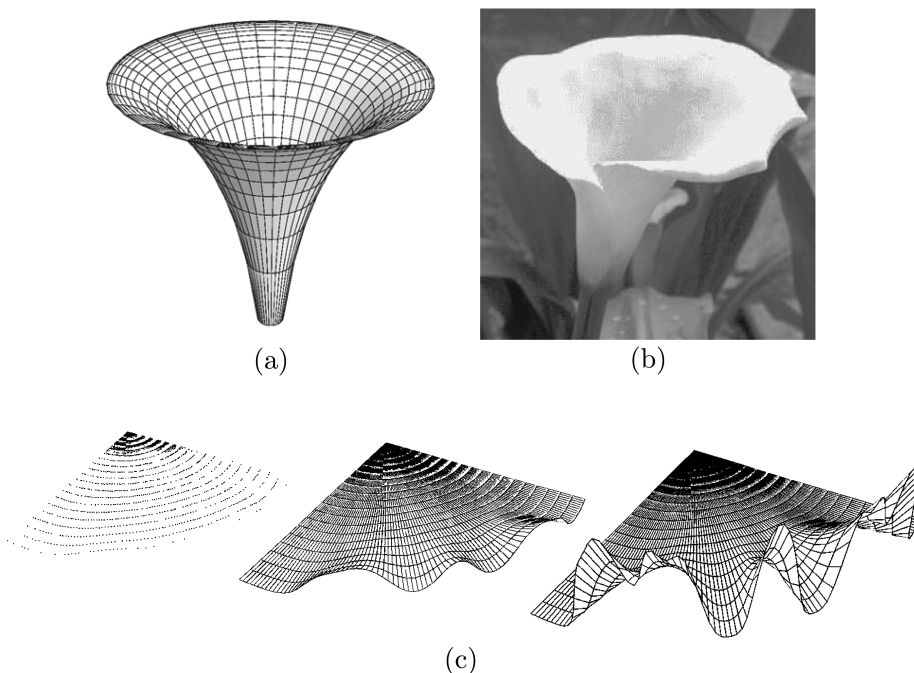
(a) (b)

(c)

FIGURE 7. (a) Pseudosphere. (b) Picture of a calla lily. (c) Sample plots of the Jacobian function encoding the Gauss curvature of the prestrain [99].

x_1 direction, localized near the $x_2 = 0$ edge of the sheet. An interesting class of buckling patterns that lower the bending energy of the sheet while satisfying the approximate isometry condition was constructed by introducing "branch point" singularities, resulting in the multiple asymptotic directions, into solutions to the Gauss curvature constraint equation, $\det \nabla^2 v = \kappa(g_{2 \times 2}) = -f''$.

For weakly hyperbolic sheets with constant $\kappa < 0$, the same construction has been recently refined in [109, 126], using a discrete differential geometric approach linked with the notion of index of topological defects, to argue that the branch points are energetically preferred and may lead to the fractal-like recursive buckling patterns seen in some flowers and leaves.

Open Problem 6.1. While we will consider the problem here solely from a static elastic perspective, it is worth asking an allied question: How does a growing front leave behind a partially relaxed shape, i.e., that of a flower?

6.1. **Weak prestrain and the Monge–Ampère constrained theories.** We assume that the given prestrain tensor $A^h = (g^h)^{1/2}$ on Ω^h is incompatible only through a perturbation of order which is a power of the film's thickness h:

$$(6.1) \qquad A^h(x', x_3) = \mathrm{Id}_3 + h^\gamma S(x') + h^{\gamma/2} x_3 B(x').$$

Here, $S, B : \bar{\omega} \to \mathbb{R}^{3\times 3}_{\text{sym}}$ are smooth tensors that correspond to stretching and bending with the choice[6] of the exponents $\gamma, \frac{\gamma}{2}$. In this context, the counterpart of Theorem 4.1 is as follows:

Theorem 6.2 ([80, 84]). *Let $u^h \in W^{1,2}(\Omega^h, \mathbb{R}^3)$ satisfy: $\mathcal{E}^h(u^h) \leq Ch^{\gamma+2}$, for some $\gamma \in (1, 2)$.*

  (i) *Compactness. There exist $R^h \in SO(3)$, $c^h \in \mathbb{R}^3$ such that the following holds for $\{y^h(x', x_3) = R^h u^h(x', hx_3) - c^h\}_{h\to 0}$. First, y^h converge to x' in $W^{1,2}(\Omega^1, \mathbb{R}^3)$. Second, the scaled displacements, $V^h(x') = \frac{1}{h^{\gamma/2}} \int_{-1/2}^{1/2} y^h(x', t) - x' \, \mathrm{d}t \in W^{1,2}(\omega, \mathbb{R}^3)$ converge, up to a subsequence, to a displacement field V of the form $V = (0, 0, v)^T$, satisfying*

(6.2) $$v \in W^{2,2}(\omega, \mathbb{R}), \qquad \det \nabla^2 v = -\operatorname{curl}\operatorname{curl} S_{2\times 2}.$$

  (ii) *Γ-convergence. If ω is simply connected with $\mathcal{C}^{1,1}$ boundary, then we have, with the same quadratic forms $\mathcal{Q}_2$ defined in (4.5),*

(6.3) $$\frac{1}{h^{\gamma+2}}\mathcal{E}^h(u^h) \xrightarrow{\Gamma} \mathcal{I}_{S,B}(v) = \frac{1}{12}\int_\omega \mathcal{Q}_2\big(x', \nabla^2 v + B_{2\times 2}\big) \, \mathrm{d}x'.$$

Similarly to Corollary 4.2, one can deduce the following.

Corollary 6.3. *The Monge–Ampère problem (6.2) has a solution $v \in W^{2,2}$ iff $\inf \mathcal{E}^h \leq Ch^{\gamma+2}$. Moreover, $ch^{\gamma+2} \leq \inf \mathcal{E}^h \leq h^{\gamma+2}$ for some $c, C > 0$ is equivalent to the solvability of (6.2) and the simultaneous nonvanishing of the lowest-order terms (i.e., terms of order γ and $\frac{\gamma}{2}$, respectively) in $\mathcal{R}_{12,12}(\cdot, 0)$ and $[\mathcal{R}_{12,i3}(\cdot, 0)]_{i=1,2}$. This last condition is equivalent to*

$$\operatorname{curl}\operatorname{curl} S_{2\times 2} + \det B_{2\times 2} \not\equiv 0 \quad or \quad \operatorname{curl} B_{2\times 2} \not\equiv 0 \quad in \ \omega.$$

Equation (6.2) can be seen as an equivalent condition for the family of deformations on ω (which, indeed, corresponds to the recovery sequence in Theorem 6.2(ii)) given through the out-of-plane displacement $v : \omega \to \mathbb{R}$, and any in-plane displacement $w : \omega \to \mathbb{R}^2$,

$$\phi^h(x') = \big(x' + h^\gamma w(x'), h^{\gamma/2} v(x')\big) : \omega \to \mathbb{R}^3$$

to match the metric $g^h(\cdot, 0)_{2\times 2}$ at the lowest-order terms of its Gauss curvature. Indeed,

(6.4)
$$\begin{aligned}
\kappa\big((\nabla\phi^h)^T\nabla\phi^h\big) &= \kappa\Big(\operatorname{Id}_2 + h^\gamma(\nabla v \otimes \nabla v + 2\operatorname{sym}\nabla w) + h^{2\gamma}(\nabla w)^T\nabla w\Big) \\
&= -\frac{h^\gamma}{2}\operatorname{curl}\operatorname{curl}\big(\nabla v \otimes \nabla v + 2\operatorname{sym}\nabla w\big) + o(h^\gamma) \\
&= h^\gamma \det \nabla^2 v + o(h^\gamma), \\
\kappa\big(g^h(\cdot, 0)_{2\times 2}\big) &= \kappa\Big(\operatorname{Id}_2 + 2h^\gamma S_{2\times 2} + h^{2\gamma}(S^2)_{2\times 2}\Big) \\
&= -h^\gamma \operatorname{curl}\operatorname{curl} S_{2\times 2} + o(h^\gamma).
\end{aligned}$$

Recalling that the kernel of the operator $\operatorname{curl}\operatorname{curl}$ consists precisely of $\operatorname{sym}\nabla w$, we further observe that (6.2) is equivalent to the possibility of choosing w such that ϕ^h is an isometric immersion of $(\omega, g^h(\cdot, 0)_{2\times 2})$ at the leading-order terms,

$$(\nabla\phi^h)^T\nabla\phi^h = \operatorname{Id}_2 + 2h^\gamma\big(\tfrac{1}{2}\nabla v \otimes \nabla v + \operatorname{sym}\nabla w\big) + \mathcal{O}(h^{2\gamma}) = g^h(\cdot, 0)_{2\times 2} + o(h^\gamma).$$

---

[6]The more general choices of exponents $\alpha/2, \gamma/2$ were analyzed in [60, 78, 79].

The above analysis suggests that we view the Monge–Ampère equation $\det \nabla^2 v = f$ through its very weak form, well defined for all $v \in W^{1,2}_{\text{loc}}(\omega, \mathbb{R})$, in the sense of distributions,

$$(6.5) \qquad \mathcal{D}et\,\nabla^2 v \doteq -\frac{1}{2}\,\text{curl curl}(\nabla v \otimes \nabla v) = f \qquad \text{in } \omega.$$

Similarly to the results described in section 4.4, one can then apply techniques of convex integration and show [18, 32, 87] that for any smooth $f : \bar{\omega} \to \mathbb{R}$ and $\alpha < \frac{1}{5}$, the set of $\mathcal{C}^{1,\alpha}(\bar{\omega})$ solutions to (6.5) is dense in $\mathcal{C}^0(\bar{\omega})$. That is, for every $v_0 \in \mathcal{C}^0(\bar{\omega})$ there exists a sequence $v_n \in \mathcal{C}^{1,\alpha}(\bar{\omega})$, converging uniformly to v_0 and satisfying $\mathcal{D}et\nabla^2 v_n = f$. One consequence of this result is that the operator $\mathcal{D}et\nabla^2$ is weakly discontinuous everywhere in $W^{1,2}(\omega)$. By an explicit construction, there follows a counterpart of Proposition 4.5:

Proposition 6.4 ([60]). *Assume that $\omega \subset \mathbb{R}^2$ is simply connected with $\mathcal{C}^{1,1}$ boundary. Then*

$$\inf \mathcal{E}^h \le Ch^\beta \qquad \text{for all } \gamma \in \left[\frac{2}{7}, 2\right] \text{ and } \beta < \frac{5}{3}\gamma + \frac{2}{3},$$

$$\inf \mathcal{E}^h \le Ch^\gamma \qquad \text{for all } \gamma \in \left(0, \frac{2}{7}\right).$$

Open Problem 6.5. Analyze the intermediate energy scaling regime $\inf \mathcal{E}^h \simeq h^\beta$ for $\beta \in \left[\frac{5}{3}\gamma + \frac{2}{3}, \gamma + 2\right)$, and find the Γ-limits of the scaled energies $\frac{1}{h^\beta}\mathcal{E}^h$.

Open Problem 6.6. Consider the generalization of (6.5) to problems posed on higher-dimensional domains $\omega \subset \mathbb{R}^N$, in the context of dimension reduction and isometry matching. As shown in [53], the set $\{\text{sym}\,\nabla w;\ W^{1,2}(\omega, \mathbb{R}^N)\}$ is the kernel of the operator Curl^2, where for $A \in L^2(\omega, \mathbb{R}^{N \times N})$ the 4-tensor, $\text{Curl}^2(A) = \left[\text{Curl}^2(A)_{ab,cd}\right]_{a,b,c,d=1\cdots N}$, is given as the application of two exterior derivatives in $\left[\partial_a\partial_c A_{bd} + \partial_b\partial_d A_{ac} - \partial_a\partial_d A_{bc} - \partial_b\partial_c A_{ad}\right]_{a,b,c,d}$. Similarly to the calculation in (6.4), there holds $\mathcal{R}_{ab,cd}(\text{Id}_N + \varepsilon^2 A) = -\frac{\varepsilon^2}{2}\,\text{Curl}^2(A)_{ab,cd} + o(\varepsilon^2)$. Taking $A = \nabla v \otimes \nabla v$, one obtains that a scalar displacement field v can be matched by a higher-order perturbation vector field w, so that defining $\bar{\phi}^h(x') = \left(x' + h^2 w(x'), hv(x')\right) : \omega \to \mathbb{R}^{N+1}$, the given weak prestrain metric is matched by the pull-back metric in $(\nabla\bar{\phi})^T\nabla\bar{\phi} = \text{Id}_N + h^2 A + \mathcal{O}(h^4)$, if and only if $\left[\det(\nabla^2 v)_{ab,cd}\right]_{a,b,c,d=1\cdots N} = -\text{Curl}^2(A)$.

6.2. Dimension reduction with transversely oscillatory prestrain.

We also mention the "oscillatory setting" where $g^h = (A^h)^2$ satisfy the structure assumption,

$$g^h(x', x_3) = \mathcal{G}^h\left(x', \frac{x_3}{h}\right) = \bar{\mathcal{G}}(x') + h\mathcal{G}_1\left(x', \frac{x_3}{h}\right) + \frac{h^2}{2}\mathcal{G}_2\left(x', \frac{x_3}{h}\right) + \cdots$$

$$\text{for all } x = (x', x_3) \in \Omega^h.$$

This setup includes the subcase $g^h = g$ of section 5 upon taking $\bar{\mathcal{G}}_1 = g(\cdot, 0)$, $\mathcal{G}_1(x', t) = t\partial_3 g(x', 0)$, $\mathcal{G}_2(x', t) = t^2\partial_{33}g(x', 0)$, etc. In [76] connections between these two cases were exhibited, via projections of appropriate curvature forms on the polynomial tensor spaces and reduction to the "effective nonoscillatory cases" in the Kirchhoff-like (h^2) and von Kármán-like (h^4) regimes. Compactness statements as in section 5.2 are then still valid, with the Γ-limits that consist of energies $\mathcal{I}_{2(n+1),\bar{g}}$

written for effective metrics $\bar{g}$, plus the new "excess term" measuring the averaged deviation of g^h from $\bar{g}$.

Open Problem 6.7. Derive the hierarchy of all the limiting theories in the oscillatory setting.

7. CLASSICAL GEOMETRICALLY NONLINEAR ELASTICITY WITHOUT PRESTRAIN

When a thin plate or shell is constrained at the boundary, it can buckle, wrinkle, or crumple depending on the nature and extent of the forcing. Similarly, when a plate or shell is subject to body forces, such as those due to gravity in such contexts as draping a complex body, the sheet again folds and wrinkles in complex ways. Examples of the resulting patterns are shown in Figure 8, and they highlight the occurrence of three constituent building blocks: extended zones of short wavelength wrinkles, strongly localized conical structures, and the ridge-like structures that can arise either together or separately from the wrinkles. What is the hierarchy of limiting elastic theories in such situations?

7.1. The setup and the finite hierarchy of Γ-limits for plates. In this section we parallel the discussion of the hierarchy of the non-Euclidean thin films presented in sections 4–6. Let $S \subset \mathbb{R}^3$ be a bounded, connected, oriented two-dimensional surface with unit normal $\vec{n}$. Consider a family $\{S^h\}_{h \to 0}$ of thin shells around the midsurface S:

$$S^h = \{x + t\vec{n}(x);\ x \in S,\ -h/2 < t < h/2\}.$$

The elastic energy (with density W that satisfies (3.2)) of a deformation $u^h : S^h \to \mathbb{R}^3$ and the total energy in presence of the applied force $f^h \in L^2(S^h, \mathbb{R}^3)$ are given, respectively, by

$$\mathcal{E}^h(u^h) = \frac{1}{h} \int_{S^h} W(\nabla u^h), \quad J^h(u^h) = \mathcal{E}^h(u^h) - \frac{1}{h} \int_{S^h} f^h u^h \quad \forall u^h \in W^{1,2}(S^h, \mathbb{R}^3).$$

It has been shown [43] that if f^h scale like h^α, then $\mathcal{E}^h(u^h)$ at approximate minimizers u^h of J^h scale like h^β, with $\beta = \alpha$ for $0 \le \alpha \le 2$ and $\beta = 2\alpha - 2$ for $\alpha > 2$. The dimension reduction question in this context consists thus of identifying the Γ-limits $\mathcal{I}_{\beta,S}$ of the rescaled energies sequence $\{\frac{1}{h^\beta} \mathcal{E}^h\}_{h \to 0}$. We stress that, contrary to the curvature-driven shape formation described in section 5, there is no energy quantization and any scaling exponent $\beta > 0$ is viable.

In case of $S \subset \mathbb{R}^2$, i.e., when $\{S^h\}_{h \to 0}$ is a family of thin plates, such Γ-convergence was first established for $\beta = 0$ [74] and later [42, 43] for all $\beta \ge 2$. This last regime corresponds to a rigid behavior of the elastic material, since the limiting deformations are isometries if $\beta = 2$ (in accordance with the general result in Theorem 4.1) or infinitesimal isometries if $\beta > 2$ (see, for example, the compactness analysis in section 5.2). One particular case is $\beta = 4$, where the derived limiting theory turns out to be the von Kármán theory (5.3). Then $\beta > 4$ with the Γ-limit as in (5.4), and $\beta \in (2, 4)$ where the result is effectively included in Theorem 6.2. We gather these results in Table 2, which should be compared with Table 1 in section 5.2.
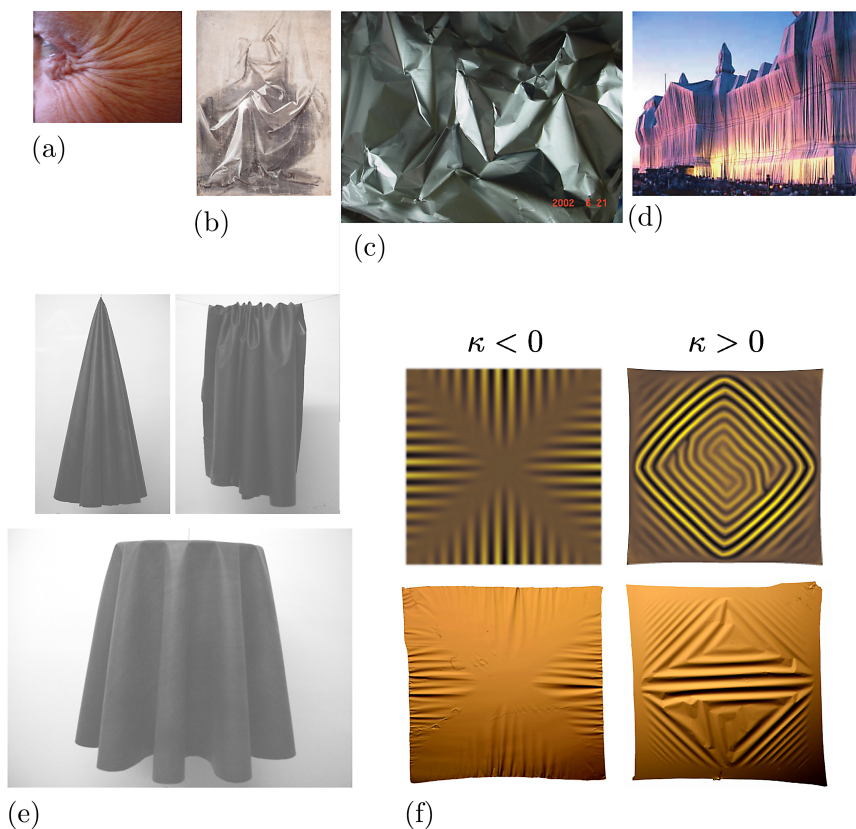
FIGURE 8. Wrinkles, drapes and crumples in thin sheets over a range of scales arise due to boundary and bulk forces. (a) Wrinkles in the neighborhood of the eye are driven by the muscular contractions. (b) The drape of a heavy piece of cloth on a knee is due to the combination of gravity and the presence of obstacles (a chiaroscuro by Leonardo). (c) The crumples in a sheet are reminiscent of the drape, but arise due to confinement, and are dominated by the present. (d) The nearly uniform wrinkles on a fabric that wraps the Reichstag in Berlin (an inspiration of the artist Christo) are due to the presence of a series of horizontal ropes; otherwise the wrinkles will coalesce into larger and larger ones. (e) The elements of all drapes are a combination of the (in)ability to drape a point (such as a tent pole), a line (such as a curve), and a curve (such as a waist or a table) in the presence of gravity [22]. (f) Complex wrinkles also arise when non-Euclidean surfaces are flattened, as shown here for a patch of a surface that is either saddle-shaped ($\kappa < 0$) or spherical ($\kappa > 0$) in its natural configuration. (Top: simulations; bottom: experiments. The images in (a)–(e) are available via Creative Commons Attribution–NonCommercial–NoDerivatives 4.0 International license. The image in (f) appears courtesy of Tobasco, Timounay, Todorova, Paulsen, and Katifori [118].)

7.2. **The infinite hierarchy of shell theories and the matching properties.**
The first result for the case when S is a surface of arbitrary geometry was given
in [74] as the membrane theory ($\beta = 0$) where the limit $\mathcal{I}_{0,S}$ depends only on the
stretching and shearing produced by the deformation. Case $\beta = 2$ was analyzed in
[41] and proved to reduce to the flexural shell model, i.e., a geometrically nonlinear
pure bending, constrained to isometric immersions of S. The energy $\mathcal{I}_{2,S}$ depends
then on the change of curvature produced by such deformation, in the same spirit
as Theorem 4.1.

For $\beta = 4$, the Γ-limit $\mathcal{I}_{4,S}$, as shown in [80–82], acts on the first-order isome-
tries $V \in \mathcal{V}_1 \cap W^{2,2}$, i.e., displacements of S whose covariant derivative is skew-
symmetric, and finite strains $B \in \mathrm{cl}_{L^2}\{\mathrm{sym}\,\nabla w;\ w \in W^{1,2}(S, \mathbb{R}^3)\}$ (compare the
definitions of spaces $\mathcal{V}_{y_0}$ and $\mathcal{S}_{y_0}$ in section 5.2). The limiting energy consists of two
terms corresponding to the stretching (second-order change in metric) and bending
(first-order change in the second fundamental form $II = \nabla \vec{N}$ on S) of a family of
deformations $\{\phi^h = \mathrm{id} + hV + h^2 w^h\}_{h \to 0}$ of S, which is induced by displacements
$V \in \mathcal{V}_1$ and w^h satisfying $\lim_{h \to 0} \mathrm{sym} \nabla w^h = B$. The out-of-plane displacements
v present in (5.3) are therefore replaced by the vector fields in $\mathcal{V}_1$ that are neither
normal nor tangential to S, but which preserve the metric on S up to first order.
For $\beta > 4$, the limiting energy consists [80, 81] only of the bending term and it
coincides with the linearly elastic flexural shell model.

The form of $\mathcal{I}_{\beta,S}$ for all $\beta > 2$ and arbitrary midsurface S has been conjectured
in [86]. Namely, $\mathcal{I}_{\beta,S}$ acts on the space of kth order infinitesimal isometries $\mathcal{V}_k$,
where k is such that

$$\beta \in [\beta_{k+1}, \beta_k) \quad \text{and} \quad \beta_n = 2 + 2/n.$$

The space $\mathcal{V}_k$ consists of k-tuples $(V_1, \ldots, V_k)$ of displacements $V_i : S \to \mathbb{R}^3$ (with
appropriate regularity), such that the deformations $\phi^\varepsilon = \mathrm{id} + \sum_{i=1}^{k} \varepsilon^i V_i$ preserve
the metric on S up to order ε^k, i.e., $(\nabla \phi^\varepsilon)^T \nabla \phi^\varepsilon - \mathrm{Id}_2 = \mathcal{O}(\varepsilon^{k+1})$. Further, setting
$\varepsilon = h^{\beta/2-1}$, we have:

(i) When $\beta = \beta_{k+1}$, then $\mathcal{I}_{\beta,S} = \int_S \mathcal{Q}_2\,(x, \delta_{k+1}I_S) + \int_S \mathcal{Q}_2\,(x, \delta_1 II_S)$, where
   $\delta_{k+1}I_S$ is the change of metric on S of the order ε^{k+1}, generated by the family
   of deformations $\{\phi^\varepsilon\}_{\varepsilon \to 0}$, and $\delta_1 II_S$ is the first-order (i.e., order ε) change in
   the second fundamental form II_S of S.

(ii) When $\beta \in (\beta_{k+1}, \beta_k)$, then $\mathcal{I}_{\beta,S} = \int_S \mathcal{Q}_2\,(x, \delta_1 II_S)$.

(iii) The constraint of kth order isometry $\mathcal{V}_k$ may be relaxed to that of $\mathcal{V}_m$, $m < k$, if
   S possesses the following $m \mapsto k$ matching property. For every $(V_1, \ldots, V_m) \in$
   $\mathcal{V}_m$ there exist sequences of corrections $V_{m+1}^\varepsilon, \ldots, V_k^\varepsilon$, uniformly bounded in ε,
   such that $\tilde{\phi}^\varepsilon = \mathrm{id} + \sum_{i=1}^{m} \varepsilon^i V_i + \sum_{i=m+1}^{k} \varepsilon^i V_i^\varepsilon$ preserve the metric on S up to
   order ε^k.

The above finding is supported by all the rigorously derived models. In partic-
ular, since plates enjoy the $2 \mapsto \infty$ matching property (i.e., as shown in [43], every
$W^{1,\infty} \cap W^{2,2}$ member of $\mathcal{V}_2$ may be matched to an exact isometry, in the sense of
(iii) above), all the plate theories for $\beta \in (2, 4)$ indeed collapse to a single theory
(linearized Kirchhoff model, see Table 2).

Further, elliptic (i.e., strictly convex up to the boundary) surfaces enjoy [82] a
matching property of $1 \mapsto \infty$, which is stronger than for the case of plates. Namely,
on S elliptic and $\mathcal{C}^{3,\alpha}$, every $V \in \mathcal{V}_1 \cap \mathcal{C}^{2,\alpha}(\bar{S})$, possesses a sequence $\{w_\varepsilon\}_{\varepsilon \to 0}$,
equibounded in $\mathcal{C}^{2,\alpha}(\bar{S}, \mathbb{R}^3)$, and such that $\phi^\varepsilon = \mathrm{id} + \varepsilon V + \varepsilon^2 w_\varepsilon$ is an (exact)

TABLE 2. The finite hierarchy of Γ-limits for plates for the energy scaling $\beta \geq 2$

scaling exponent β	asymptotic expansion of minimizing $u^h_{|\omega}$	constraint / regularity	Γ−limit $\mathcal{I}_{\beta,S}$
$\beta = 2$ Kirchhoff	$y(x')$ $\{3d: \ y(x') + x_3\vec{n}(x')\}$	$y \in W^{2,2}(\omega, \mathbb{R}^3)$ $(\nabla y)^T\nabla y = \mathrm{Id}_2$	$c\|(\nabla y)^T\nabla\vec{N}\|^2_{\mathcal{Q}_2}$
$2 < \beta < 4$ linearized Kirchhoff	$x' + h^{\beta/2-1}v(x')x_3$	$v \in W^{2,2}(\omega, \mathbb{R})$ $\det\nabla^2 v = 0$	$c\|\nabla^2 v\|^2_{\mathcal{Q}_2}$
$\beta = 4$ von Kármán	$x' + hv(x')x_3$ $+h^2w(x')$	$v \in W^{2,2}(\omega, \mathbb{R})$ $w \in W^{1,2}(\omega, \mathbb{R}^2)$	$c_1\|\frac{1}{2}\nabla v^{\otimes 2} + (\nabla w)_{\mathrm{sym}}\|^2_{\mathcal{Q}_2}$ $+c_2\|\nabla^2 v\|^2_{\mathcal{Q}_2}$
$\beta > 4$ linear elasticity	$x' + h^{\beta/2-1}v(x')x_3$	$v \in W^{2,2}(\omega, \mathbb{R})$	$c\|\nabla^2 v\|^2_{\mathcal{Q}_2}$

isometry for all $\varepsilon \ll 1$. Regarding the assumed regularity of V (which is higher than the expected regularity $W^{2,2}$ of a limiting displacement), we note that the usual mollification techniques do not guarantee the density of smooth infinitesimal isometries in $\mathcal{V}_1 \cap W^{2,2}$, even for $S \in \mathcal{C}^\infty$. However, a density result is valid for elliptic $S \in \mathcal{C}^{m+2,\alpha}$; that is, for every $V \in \mathcal{V}_1 \cap W^{2,2}$ there exists a sequence $\{V_n \in \mathcal{V}_1 \cap \mathcal{C}^{m,\alpha}(\bar{S}, \mathbb{R}^3)\}_{n \to \infty}$ such that $\lim_{n\to\infty}\|V_n - V\|_{W^{2,2}(S)} = 0$. The proof of the quoted results adapts techniques used for showing immersability of all positive curvature metrics on a sphere [52]. As a consequence, for elliptic surfaces with sufficient regularity, the Γ-limit of the nonlinear elastic energies $h^{-\beta}\mathcal{E}^h$ for any scaling regime $\beta > 2$ is given by the bending functional constrained to the first-order isometries, as in the case $\beta > 4$.

In [56, 57] matching and density properties of isometries on developable surfaces without affine regions has been proved. Namely, on such S of regularity $\mathcal{C}^{2k,1}$, every $V \in \mathcal{V}_1 \cap \mathcal{C}^{2k-1,1}$ enjoys $1 \mapsto k$ matching property. Further, the space $\mathcal{V}_1 \cap \mathcal{C}^{2k-1}$ is dense in $\mathcal{V}_1$. The implication for elasticity of thin shells with smooth developable midsurface is that, again, the only small slope theory is the linear theory—a developable shell transitions directly from the linear regime to fully nonlinear bending if the applied forces are adequately increased. While the von Kármán theory describes buckling of thin plates, the equivalent variationally correct theory for developable shells is the purely nonlinear bending. It is worth noting that the class of developable shells includes smooth cylinders which are ubiquitous in nature and technology over a range of length scales. An example of a recently discovered structure is carbon nanotubes, i.e., molecular-scale tubes of graphitic carbon with outstanding rigidity properties—they are among the stiffest materials in terms of the tensile strength and elastic modulus, but they easily buckle under compressive, torsional, or bending stress.

Open Problem 7.1. Investigate the matching properties for other types of surfaces.

8. Future directions

Our review on the mathematical aspects of the morphogenesis and pattern formation in thin sheets has focused on low-dimensional shapes that arise from inhomogeneous growth and/or boundary conditions and constraints. From a biological

perspective, understanding how growth leads to shape is only half the problem. A true understanding of morphogenesis also requires understanding how shape feeds back to growth, to ultimately regulate shape and thus enable function. From a technological perspective, an equally interesting problem is the inverse problem: How should one prescribe the growth patterns in order to be able to convert a flat sheet into a complex landscape, a flower, or even a face?

From an artistic perspective, a natural generalization of the questions on the smoothness of and in pattern-forming elastic surfaces is that posed by the ancient Sino-Japanese paper arts of origami and kirigami (from the japanese: oru = fold, $kiri$ = cut, $kami$ = paper): What are the limits to the shapes that one can construct with sharp folds and cuts that violate smoothness along cuts and creases (either straight or curved)? Artists have long known how to fold a sheet into a crane, a man, or a dragon, and how to use cuts to articulate a sheet so that it can be made into a pop-up castle or a rose. How can one quantify these art forms as inverse problems in discrete geometry and topology? We touch on each of these three problems briefly to highlight recent progress and the many open problems that remain.

8.1. Developmental feedback from shape to growth.

In a biological context, there is increasing evidence for a mechanical feedback loop linking shape back to growth [59, 110]; i.e., the growth tensors associated with causing shape are themselves affected by shape. To quantify how growth patterns change in response to shape in space and time with (unknown) kernels that characterize the nature of this feedback, one must turn to experiments. Nevertheless, it might still be useful to study simple feedback laws to understand their mathematical consequences as has been recently attempted in the context of controlling bacterial shapes [2]. A minimal example of a local model, incorporating mechanical feedback in tissue growth (in such instances as leaves and epithelial tissues), that closes the equations (2.1), takes the form

$$
\begin{aligned}
(8.1) \quad \alpha_v \Delta(\operatorname{tr} \dot{\mathbf{s}}) &= -\alpha \Delta(\operatorname{tr} \mathbf{s}) - \frac{\alpha}{2} \det(\boldsymbol{\kappa}_0 - \boldsymbol{\kappa}) - \Delta[\operatorname{tr}(\boldsymbol{\sigma}_0 - \boldsymbol{\sigma})] - \beta_v \Delta(\operatorname{tr} \dot{\mathbf{b}}) \\
&= -\beta \Delta(\operatorname{tr} \mathbf{b}) - \beta \Delta[\operatorname{tr}(\boldsymbol{\kappa}_0 - \boldsymbol{\kappa})] + \operatorname{tr}[(\boldsymbol{\sigma}_0 - \boldsymbol{\sigma})(\boldsymbol{\kappa}_0 - \boldsymbol{\kappa})]
\end{aligned}
$$

for the dynamics of in-plane growth and curvature tensors $\mathbf{s}, \mathbf{b}$, respectively. Here, the terms $\boldsymbol{\sigma}_0, \boldsymbol{\kappa}_0$ denote the threshold homeostatic values of the stress tensor $\boldsymbol{\sigma}$ and the curvature tensor $\boldsymbol{\kappa}$ that the tissue aims to achieve, and the various prefactors are as defined in the introductory section, except for α_v, β_v which are the stretching viscosity and bending viscosity, respectively, with $\alpha_v/\alpha = \tau_S, \beta_v/\beta = \tau_B$ being the time scale for the relaxation of in-plane and out-of-plane growth. We note that these equations are linear in $\mathbf{s}, \mathbf{b}$ and thus are likely to be valid only in the neighborhood of homeostatic stress and curvature.

Open Problem 8.1. System (8.1) is geometrically nonlinear. What are the conditions for its dynamic stability and control of the equilibrium states, which result from inhomogeneous and anisotropic growth?

Other possible descriptions were suggested in [7, 16, 48, 83, 108]. In particular, the paper [16] has recently introduced a free boundary problem for a system of PDEs modeling growth. There, a morphogen controlling volume growth and produced by specific cells was assumed to be diffused and absorbed throughout the domain, whose geometric shape was in turn determined by the instantaneous minimization

FIGURE 9. Examples of solutions of inverse problems in morphogenesis—to program the metric structure and thence create complex shapes from flat sheets. On the left are shown experiments with 3d printed gel structures that swell in a good solvent, along with representative numerical solutions that are based on minimizing the energy (4.1). (This figure is from [47] by Gladman, Matsumoto, Nuzzo, Mahadevan, and Lewis, *Biomimetic 4D printing*, Nature–Materials, **15** (2016), 413–418; © 2018, Springer Nature.) On the right [120] we see results of the solution of inverse problems to grow a flower from a bilayer cylindrical shell, and a face from a circular bilayer disk.

of an elastic deformation energy, subject to a constraint on the volumetric growth. For an initial domain with $\mathcal{C}^{2,\alpha}$ regular boundary, it establishes the local existence and uniqueness of a classical solution, up to a rigid motion.

8.2. **Inverse problems in morphogenesis.** With the advent of additive manufacturing methods such as 3d and 4d printing (to account for variations in space and time), it has now become possible to print planar patterns of responsive inks that swell or shrink inhomogeneously when subject to light, pH, humidity, etc., thus causing them to bend and twist out of the plane [14, 47]. Understanding how to design the ink materials and the geometric print paths to vary the density and anisotropy of the print patterns in a monolayer or a bilayer is critical to enable functional patterns. This inverse design problem requires the specification of the first and second fundamental form which will not generally be compatible with a strain-free final shape. Recent work in this area [120] shows that a way around this is to use a bilayer with independent control over the two layers, and it leads to results such as those shown in Figure 9. A related class of design problems in solid mechanics, leading to a variation on the classical question of equidimensional embeddability of Riemannian manifolds, has been addressed in [1].

8.3. **Discrete problems: Origami and kirigami.** Origami is the art of folding paper along sharp creases to create complex three-dimensional shapes, and thus it is more amenable to the methods of discrete geometry. A natural question here is that of designing the number, location, and orientation of folds on a flat sheet of paper and prescribing the order of folding to achieve a given target shape. For a prescribed fold topology (e.g., that of 4-coordinated vertices), geometric rules that quantify the constraints of local length, angle, and area preservation allow one to pose the inverse problem of fold design as a constrained optimization problem [37, 38, 123]. Then, given reasonable initial states, one can determine the folding patterns to achieve target shapes (see Figure 10) that are realized as spatially modulated patterns of a simple periodic and uniform tiling, yielding approximations to given surfaces of constant or varying curvature, and which are corroborated using experiments with paper. The difficulty of realizing these geometric structures may be assessed by quantifying the energetic barrier that separates the metastable flat and folded states. The trade-off between the accuracy to which the pattern conforms to the target surface and the effort associated with creating finer folds can also be characterized [34]. However, there are a host of mathematical problems that remain open. These include the presence (or absence) of impossibility theorems on what shapes can or cannot be achieved using folds in a sheet of paper and the consequences of fold topology on the resulting shapes.

Open Problem 8.2. How can one control the rigidity of a randomly origamized sheet as the number of random creases is gradually increased, and the sheet is subjected to the geometric rules that the creases must satisfy at every vertex (i.e., the sum of all angles must add up to $2\pi^c$, and that alternate angles must add up to π^c [38])?

Kirigami is the art of cutting paper to make it articulated and deployable. The mechanical response of a kirigami sheet when it is pulled at its ends is enabled and limited by the presence of cuts that serve to guide the possible nonplanar deformations. Recently, this ability has become the inspiration for a new class of mechanical metamaterials [11, 17]. The geometrical and topological properties of the slender sheet-like structures, irrespective of their material constituents, were exploited to discuss functional structures on scales ranging from the nanometric [13] to centimetric and beyond [25, 26, 103].

A combination of physical and numerical experiments can be used to characterize the geometric mechanics of kirigamized sheets as a function of the number, size, and orientation of cuts [24]. Of particular interest is understanding how varying the the shortest path between points at which forces are applied, influences the shape of the deployment of the trajectory of a sheet as well as how to control its compliance across orders of magnitude.

Mathematically, these questions are related to the nature and form of geodesics in the Euclidean plane with linear obstructions (cuts) and to the nature and form of isometric immersions of the sheet with cuts when it can be folded on itself. In [54], a constructive proof has been provided that the geodesic connecting any two points in the sheet is piecewise polygonal, and that the family of all such geodesics can be simultaneously rectified into a straight line by flat-folding the sheet so that its configuration is a (nonunique) piecewise affine isometric immersion.
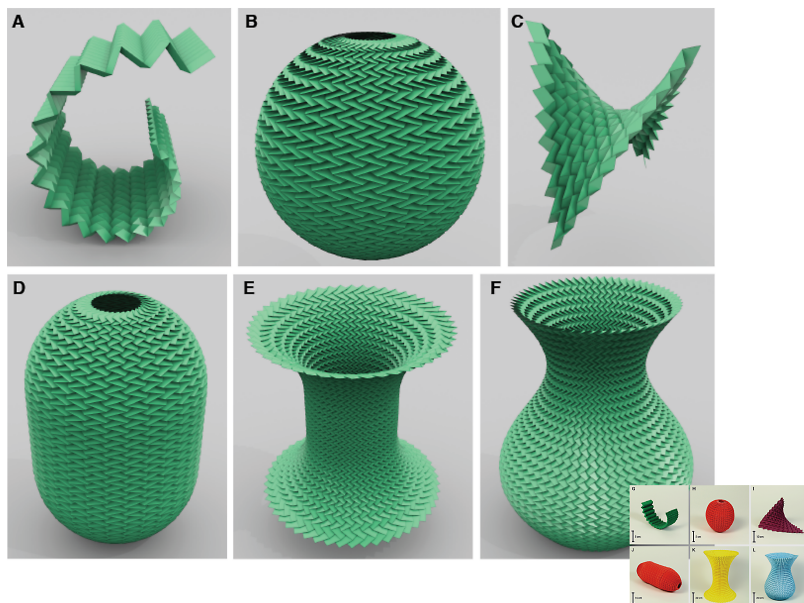
FIGURE 10. While this paper has focused on surfaces with varying degrees of smoothness, an interesting new avenue for exploration is that of discrete surfaces [38] that have strongly creased regions, seen for example in origami. (This figure appeared in [38], Dudte, Bouga, Tachi, and Mahadevan, *Programming curvature using origami tessellations*, Nature–Materials, **15** (2016), no. 5, 583–588; © 2016, Springer Nature.)

Open Problem 8.3. Study the structure of geodesics in the kirigamized sheet as the number of random cuts increases to infinity and under various assumptions on the cuts' distribution. What is the Hausdorff dimension of the limiting paths?

ABOUT THE AUTHORS

Marta Lewicka is a mathematician specializing in mathematical analysis and partial differential equations. She has contributed results in the theory of hyperbolic systems of conservation laws, fluid dynamics, calculus of variations, nonlinear potential theory, and differential games. She is a Fellow of the American Mathematical Society, and holds Professor's scientific title awarded by the President of the Republic of Poland. She is associate professor of mathematics at the University of Pittsburgh.

L. Mahadevan is the de Valpine Professor of Applied Mathematics, Physics, and Organismic and Evolutionary Biology at Harvard University, where he also serves as the Faculty Dean of Mather House, one of twelve undergraduate houses at Harvard College. His interests are in using experiments, theory, and computations to understand motion and matter at the observable scale of "middle earth", a fertile playground of rich phenomena spanning the physical and biological sciences that are easy to observe yet not always easy to explain. He is a MacArthur Fellow and a Fellow of the Royal Society.

References

[1] A. Acharya, M. Lewicka, and M. R. Pakzad, *The metric-restricted inverse design problem*, Nonlinearity **29** (2016), no. 6, 1769–1797, DOI 10.1088/0951-7715/29/6/1769. MR3502228

[2] S. Al Mosleh, A. Gopinathan, C. Santangelo, *Growth of form in thin elastic structures*, Soft Matter, **14** (2018), no. 41, 8361–8371.

[3] M. Arroyo and A. DeSimone, *Shape control of active surfaces inspired by the movement of euglenids*, J. Mech. Phys. Solids **62** (2014), 99–112, DOI 10.1016/j.jmps.2013.09.017. MR3131810

[4] B. Audoly and A. Boudaoud, *Self-similar structures near boundaries in strained systems*, Phys. Rev. Lett., **91**, 086105, (2004).

[5] P. Bella and R. V. Kohn, *Metric-induced wrinkling of a thin elastic sheet*, J. Nonlinear Sci. **24** (2014), no. 6, 1147–1176, DOI 10.1007/s00332-014-9214-9. MR3275221

[6] P. Bella and R. V. Kohn, *Coarsening of folds in hanging drapes*, Comm. Pure Appl. Math. **70** (2017), no. 5, 978–1021, DOI 10.1002/cpa.21643. MR3628880

[7] M. Ben Amar and A. Goriely, *Growth and instability in elastic tissues*, J. Mech. Phys. Solids **53** (2005), no. 10, 2284–2319, DOI 10.1016/j.jmps.2005.04.008. MR2167636

[8] M. Ben Amar, M. M. Müller, and M. Trejo, *Petal shapes of sympetalous flowers: the interplay between growth, geometry and elasticity*, New J. Physics, **14** (2012), 085014.

[9] H. Ben Belgacem, S. Conti, A. DeSimone, and S. Müller, *Rigorous bounds for the Föppl–von Kármán theory of isotropically compressed plates*, J. Nonlinear Sci. **10** (2000), no. 6, 661–683, DOI 10.1007/s003320010007. MR1799395

[10] H. Ben Belgacem, S. Conti, A. DeSimone, and S. Müller, *Energy scaling of compressed elastic films—three-dimensional elasticity and reduced theories*, Arch. Ration. Mech. Anal. **164** (2002), no. 1, 1–37, DOI 10.1007/s002050200206. MR1921161

[11] K. Bertoldi, V. Vitelli, J. Christensen, and M. Van Hecke, *Flexible mechanical metamaterials*, Nature Reviews Materials, **2** (2017), no. 11, 1–11.

[12] K. Bhattacharya, M. Lewicka, and M. Schäffner, *Plates with incompatible prestrain*, Arch. Ration. Mech. Anal. **221** (2016), no. 1, 143–181, DOI 10.1007/s00205-015-0958-7. MR3483893

[13] M. K. Blees, A. W. Barnard, P. A. Rose, S. P. Roberts, K. L. McGill, P. Y. Huang, A. R. Ruyack, J. W. Kevek, B. Kobrin, D. A. Muller, and P. L. McEuen, *Graphene kirigami*, Nature, **524** (2015), no. 7564, 204–207.

[14] J. W. Boley, W. Van Rees, C. Lissandrello, M. Horenstein, R. Truby, A. Kotikian, J. Lewis, and L. Mahadevan, *Shape-shifting structured lattices via multimaterial 4D printing*, Proceedings of the National Academy of Sciences, **116** (2019), no. 42, 20856–20862.

[15] Ju. F. Borisov, $C^{1,\alpha}$*-isometric immersions of Riemannian spaces* (Russian), Dokl. Akad. Nauk SSSR **163** (1965), 11–13. MR0192449

[16] A. Bressan and M. Lewicka, *A model of controlled growth*, Arch. Ration. Mech. Anal. **227** (2018), no. 3, 1223–1266, DOI 10.1007/s00205-017-1183-3. MR3744385

[17] S. Callens and A. Zadpoor, *From flat sheets to curved geometries: Origami and kirigami approaches*, Materials Today, **21** (2018), no. 3, 241–264.

[18] W. Cao and L. Székelyhidi, *Very weak solutions to the two-dimensional Monge-Ampère equation*, Sci. China Math. **62** (2019), no. 6, 1041–1056, DOI 10.1007/s11425-018-9516-7. MR3951880

[19] E. Cerda, S. Chaieb, F. Melo, and L. Mahadevan, *Conical dislocations in crumpling*, Nature, **401** (1999), no. 6748, 46–49.

[20] E. Cerda and L. Mahadevan, *Conical surfaces and crescent singularities in crumpled sheets*, Physical Review Letters, **80** (1998), no. 11, 2358.

[21] E. Cerda and L. Mahadevan, *Confined developable elastic surfaces: cylinders, cones and the Elastica*, Proc. R. Soc. Lond. Ser. A Math. Phys. Eng. Sci. **461** (2005), no. 2055, 671–700, DOI 10.1098/rspa.2004.1371. MR2121930

[22] E. Cerda, L. Mahadevan, and J. M. Pasini, *The elements of draping*, Proc. Natl. Acad. Sci. USA **101** (2004), no. 7, 1806–1810, DOI 10.1073/pnas.0307160101. MR2033755

[23] E. Cerda, K. Ravi-Chandar, and L. Mahadevan, *Wrinkling of a stretched elastic sheet*, Nature, **419** (2002), 579.

[24] G. Chaudhary, L. Niu, M. Lewicka, Q. Han, and L. Mahadevan, *Geometric mechanics of random kirigami*, in preparation, 2021.

[25] Choi, G.P., Dudte, L.H., Mahadevan, L., *Programming shape using kirigami tesselations*, Nat. Materials **18** (2019), 999-1004.

[26] Choi, G.P., Dudte, L.H., Mahadevan, L., *Compact reconfigurable kirigami*, `arXiv:2012.09241`, 2020.

[27] P. G. Ciarlet, *Mathematical elasticity. Vols. I–III*, Studies in Mathematics and its Applications, vol. 20, North-Holland Publishing Co., Amsterdam, 1988. Three-dimensional elasticity. MR936420

[28] S. Conti, C. De Lellis, and L. Székelyhidi Jr., *h-principle and rigidity for $C^{1,\alpha}$ isometric embeddings*, Nonlinear partial differential equations, Abel Symp., vol. 7, Springer, Heidelberg, 2012, pp. 83–116, DOI 10.1007/978-3-642-25361-4_5. MR3289360

[29] S. Conti and F. Maggi, *Confining thin elastic sheets and folding paper*, Arch. Ration. Mech. Anal. **187** (2008), no. 1, 1–48, DOI 10.1007/s00205-007-0076-2. MR2358334

[30] G. Dal Maso, *An introduction to Γ-convergence*, Progress in Nonlinear Differential Equations and their Applications, vol. 8, Birkhäuser Boston, Inc., Boston, MA, 1993, DOI 10.1007/978-1-4612-0327-8. MR1201152

[31] C. De Lellis and D. Inauen, *$C^{1,\alpha}$ isometric embeddings of polar caps*, Adv. Math. **363** (2020), 106996, 39, DOI 10.1016/j.aim.2020.106996. MR4054053

[32] C. De Lellis, D. Inauen, and L. Székelyhidi Jr., *A Nash–Kuiper theorem for $C^{1,1/5-\delta}$ immersions of surfaces in 3 dimensions*, Rev. Mat. Iberoam. **34** (2018), no. 3, 1119–1152, DOI 10.4171/RMI/1019. MR3850282

[33] C. De Lellis and L. Székelyhidi Jr., *High dimensionality and h-principle in PDE*, Bull. Amer. Math. Soc. (N.S.) **54** (2017), no. 2, 247–282, DOI 10.1090/bull/1549. MR3619726

[34] E. D. Demaine and J. O'Rourke, *Geometric folding algorithms*: *Linkages, origami, polyhedra*, Cambridge University Press, Cambridge, 2007, DOI 10.1017/CBO9780511735172. MR2354878

[35] J. Dervaux and M. Ben Amar, *Morphogenesis of growing soft tissues*, Phys. Rev. Lett., **101** (2008), 068101.

[36] J. Dervaux, P. Ciarletta, and M. Ben Amar, *Morphogenesis of thin hyperelastic plates: a constitutive theory of biological growth in the Föppl–von Kármán limit*, J. Mech. Phys. Solids **57** (2009), no. 3, 458–471, DOI 10.1016/j.jmps.2008.11.011. MR2500622

[37] M. A. Dias, L. H. Dudte, L. Mahadevan, and C. D. Santangelo, *Geometric mechanics of curved crease origami*, Phys. Rev. Lett., **109** (2012), 114301.

[38] L. Dudte, E. Vouga, T. Tachi, and L. Mahadevan, *Programming curvature using origami tessellations*, Nature Materials, **15** (2016), no. 5, 583–588.

[39] K. Efimenko, M. Rackaitis, E. Manias, A. Vaziri, L. Mahadevan, and J. Genzer, *Self-similar nested wrinkling patterns in skins*, Nature—Materials, **4** (2005), 293–97.

[40] E. Efrati, E. Sharon, and R. Kupferman, *Elastic theory of unconstrained non-Euclidean plates*, J. Mech. Phys. Solids **57** (2009), no. 4, 762–775, DOI 10.1016/j.jmps.2008.12.004. MR2510285

[41] G. Friesecke, R. D. James, M. G. Mora, and S. Müller, *Derivation of nonlinear bending theory for shells from three-dimensional nonlinear elasticity by Gamma-convergence* (English, with English and French summaries), C. R. Math. Acad. Sci. Paris **336** (2003), no. 8, 697–702, DOI 10.1016/S1631-073X(03)00028-1. MR1988135

[42] G. Friesecke, R. D. James, and S. Müller, *A theorem on geometric rigidity and the derivation of nonlinear plate theory from three-dimensional elasticity*, Comm. Pure Appl. Math. **55** (2002), no. 11, 1461–1506, DOI 10.1002/cpa.10048. MR1916989

[43] G. Friesecke, R. D. James, and S. Müller, *A hierarchy of plate models derived from nonlinear elasticity by gamma-convergence*, Arch. Ration. Mech. Anal. **180** (2006), no. 2, 183–236, DOI 10.1007/s00205-005-0400-7. MR2210909

[44] G. Gemmer, E. Sharon, T. Shearman, and S. Venkataramani, *Isometric immersions, energy minimization and self-similar buckling in non-Euclidean elastic sheets*, EPL, **114** (2016), 24003.

[45] J. A. Gemmer and S. C. Venkataramani, *Shape selection in non-Euclidean plates*, Phys. D **240** (2011), no. 19, 1536–1552, DOI 10.1016/j.physd.2011.07.002. MR2842894

[46] Gemmer, J., Venkataramani, S., *Shape transitions in hyperbolic non-Euclidean plates*, Soft Matter, **34** (2013), 8151-8161.

[47] A. Gladman, E. Matsumoto, R. Nuzzo, L. Mahadevan, and J. Lewis, *Biomimetic 4D printing*, Nature Materials, **15** (2016), 413–418.

[48] A. Goriely, *The mathematics and mechanics of biological growth*, Interdisciplinary Applied Mathematics, vol. 45, Springer, New York, 2017, DOI 10.1007/978-0-387-87710-5. MR3585488

[49] E. Grinspun, A. Hirani, M. Desbrun, and P. Schröder, *Discrete shells*, In Proceedings of the 2003 ACM SIGGRAPH/Eurographics symposium on Computer animation, pp. 62–67, (2003).

[50] M. Gromov, *Partial differential relations*, Ergebnisse der Mathematik und ihrer Grenzgebiete (3) [Results in Mathematics and Related Areas (3)], vol. 9, Springer-Verlag, Berlin, 1986, DOI 10.1007/978-3-662-02267-2. MR864505

[51] P. Guan and Y. Y. Li, *The Weyl problem with nonnegative Gauss curvature*, J. Differential Geom. **39** (1994), no. 2, 331–342. MR1267893

[52] Q. Han and J.-X. Hong, *Isometric embedding of Riemannian manifolds in Euclidean spaces*, Mathematical Surveys and Monographs, vol. 130, American Mathematical Society, Providence, RI, 2006, DOI 10.1090/surv/130. MR2261749

[53] Q. Han and M. Lewicka, *Convex integration for the Monge-Ampère systems*, in preparation, 2021.

[54] Q. Han, M. Lewicka, and L. Mahadevan, *Geodesics and isometric immersions in kirigami*, submitted, 2021.

[55] J. Hong and C. Zuily, *Isometric embedding of the 2-sphere with nonnegative curvature in* $\mathbf{R}^3$, Math. Z. **219** (1995), no. 3, 323–334, DOI 10.1007/BF02572368. MR1339708

[56] P. Hornung, *Continuation of infinitesimal bendings on developable surfaces and equilibrium equations for nonlinear bending theory of plates*, Comm. Partial Differential Equations **38** (2013), no. 8, 1368–1408, DOI 10.1080/03605302.2013.795967. MR3169749

[57] P. Hornung, M. Lewicka, and M. R. Pakzad, *Infinitesimal isometries on developable surfaces and asymptotic theories for thin developable shells*, J. Elasticity **111** (2013), no. 1, 1–19, DOI 10.1007/s10659-012-9391-4. MR3023590

[58] J. A. Iaia, *Isometric embeddings of surfaces with nonnegative curvature in* $\mathbf{R}^3$, Duke Math. J. **67** (1992), no. 2, 423–459, DOI 10.1215/S0012-7094-92-06717-2. MR1177314

[59] K. D. Irvine and B. I. Shraiman, *Mechanical control of growth: ideas, facts and challenges*, Development, **144** (2017), no. 23, 4238–4248.

[60] S. J. Bolaños and M. Lewicka, *Dimension reduction for thin films prestrained by shallow curvature*, Proc. A. **477** (2021), no. 2247, Paper No. 20200854, 24. MR4247253

[61] W. Jin and P. Sternberg, *Energy estimates for the von Kármán model of thin-film blistering*, J. Math. Phys. **42** (2001), no. 1, 192–199, DOI 10.1063/1.1316058. MR1808773

[62] R. Kempaiah and Z. Nie, *From nature to synthetic systems: shape transformation in soft materials*, J. Mater. Chem. B, **2** (2014), 2357–2368.

[63] J. Kim, J. A. Hanna, M. Byun, C. D. Santangelo, and R. C. Hayward, *Designing responsive buckled surfaces by halftone gel lithography*, Science **335** (2012), no. 6073, 1201–1205, DOI 10.1126/science.1215309. MR2934634

[64] Y. Klein, E. Efrati, and E. Sharon, *Shaping of elastic sheets by prescription of non-Euclidean metrics*, Science **315** (2007), no. 5815, 1116–1120, DOI 10.1126/science.1135994. MR2290671

[65] Y. Klein, S. Venkataramani, and E. Sharon, *Experimental study of shape transitions and energy scaling in thin non-Euclidean plates*, Phys. Rev. Lett., **106** (2011), 118303.

[66] M. Koehl, W. K. Silk, H. Y. Liang, and L. Mahadevan, *How kelp produce blade shapes suited to different flow regimes: A new wrinkle*, Integ. and Comp. Biol., **48** (2008), 834–851.

[67] R. V. Kohn and E. O'Brien, *On the bending and twisting of rods with misfit*, J. Elasticity **130** (2018), no. 1, 115–143, DOI 10.1007/s10659-017-9635-4. MR3738374

[68] R. V. Kohn and E. O'Brien, *The wrinkling of a twisted ribbon*, J. Nonlinear Sci. **28** (2018), no. 4, 1221–1249, DOI 10.1007/s00332-018-9447-0. MR3817781

[69] N. H. Kuiper, *On* C^1*-isometric imbeddings. I, II*, Nederl. Akad. Wetensch. Proc. Ser. A. **58** = Indag. Math. **17** (1955), 545–556, 683–689. MR0075640

[70] R. Kupferman and C. Maor, *A Riemannian approach to the membrane limit in non-Euclidean elasticity*, Commun. Contemp. Math. **16** (2014), no. 5, 1350052, 34, DOI 10.1142/S0219199713500521. MR3253899

[71] R. Kupferman and J. P. Solomon, *A Riemannian approach to reduced plate, shell, and rod theories*, J. Funct. Anal. **266** (2014), no. 5, 2989–3039, DOI 10.1016/j.jfa.2013.09.003. MR3158716

[72] R. Kupferman and Y. Shamai, *Incompatible elasticity and the immersion of non-flat Riemannian manifolds in Euclidean space*, Israel J. Math. **190** (2012), 135–156, DOI 10.1007/s11856-011-0187-1. MR2956236

[73] E. H. Lee, *Elastic-plastic deformation at finite strains*, ASME J. Appl. Mech., **36** (1969), 1–6.

[74] H. Le Dret and A. Raoult, *The membrane shell model in nonlinear elasticity: a variational asymptotic derivation*, J. Nonlinear Sci. **6** (1996), no. 1, 59–84, DOI 10.1007/s003329900003. MR1375820

[75] M. Lewicka, *Quantitative immersability of Riemann metrics and the infinite hierarchy of prestrained shell models*, Arch. Ration. Mech. Anal. **236** (2020), no. 3, 1677–1707, DOI 10.1007/s00205-020-01500-y. MR4076073

[76] M. Lewicka and D. Lučić, *Dimension reduction for thin films with transversally varying prestrain: oscillatory and nonoscillatory cases*, Comm. Pure Appl. Math. **73** (2020), no. 9, 1880–1932, DOI 10.1002/cpa.21871. MR4156611

[77] M. Lewicka, L. Mahadevan, and M. R. Pakzad, *The Föppl–von Kármán equations for plates with incompatible strains*, Proc. R. Soc. Lond. Ser. A Math. Phys. Eng. Sci. **467** (2011), no. 2126, 402–426, DOI 10.1098/rspa.2010.0138. With supplementary data available online. MR2748099

[78] M. Lewicka, L. Mahadevan, and R. Pakzad, *Models for elastic shells with incompatible strains*, Proceedings of the Royal Society A, **470** (2014), 20130604.

[79] M. Lewicka, L. Mahadevan, and M. R. Pakzad, *The Monge-Ampère constraint: matching of isometries, density and regularity, and elastic theories of shallow shells* (English, with English and French summaries), Ann. Inst. H. Poincaré Anal. Non Linéaire **34** (2017), no. 1, 45–67, DOI 10.1016/j.anihpc.2015.08.005. MR3592678

[80] M. Lewicka, M. G. Mora, and M. R. Pakzad, *A nonlinear theory for shells with slowly varying thickness* (English, with English and French summaries), C. R. Math. Acad. Sci. Paris **347** (2009), no. 3-4, 211–216, DOI 10.1016/j.crma.2008.12.017. MR2538115

[81] M. Lewicka, M. G. Mora, and M. R. Pakzad, *Shell theories arising as low energy Γ-limit of 3d nonlinear elasticity*, Ann. Sc. Norm. Super. Pisa Cl. Sci. (5) **9** (2010), no. 2, 253–295. MR2731157

[82] M. Lewicka, M. G. Mora, and M. R. Pakzad, *The matching property of infinitesimal isometries on elliptic surfaces and elasticity of thin shells*, Arch. Ration. Mech. Anal. **200** (2011), no. 3, 1023–1050, DOI 10.1007/s00205-010-0387-6. MR2796137

[83] M. Lewicka and P. B. Mucha, *A local and global well-posedness results for the general stress-assisted diffusion systems*, J. Elasticity **123** (2016), no. 1, 19–41, DOI 10.1007/s10659-015-9545-2. MR3456950

[84] M. Lewicka, P. Ochoa, and M. R. Pakzad, *Variational models for prestrained plates with Monge-Ampère constraint*, Differential Integral Equations **28** (2015), no. 9-10, 861–898. MR3360723

[85] M. Lewicka and M. R. Pakzad, *Scaling laws for non-Euclidean plates and the $W^{2,2}$ isometric immersions of Riemannian metrics*, ESAIM Control Optim. Calc. Var. **17** (2011), no. 4, 1158–1173, DOI 10.1051/cocv/2010039. MR2859870

[86] M. Lewicka and M. R. Pakzad, *The infinite hierarchy of elastic shell models: some recent results and a conjecture*, Infinite dimensional dynamical systems, Fields Inst. Commun., vol. 64, Springer, New York, 2013, pp. 407–420, DOI 10.1007/978-1-4614-4523-4_16. MR2986945

[87] M. Lewicka and M. R. Pakzad, *Convex integration for the Monge-Ampère equation in two dimensions*, Anal. PDE **10** (2017), no. 3, 695–727, DOI 10.2140/apde.2017.10.695. MR3641884

[88] M. Lewicka, A. Raoult, and D. Ricciotti, *Plates with incompatible prestrain of high order*, Ann. Inst. H. Poincaré Anal. Non Linéaire **34** (2017), no. 7, 1883–1912, DOI 10.1016/j.anihpc.2017.01.003. MR3724760

[89] H. Liang and L. Mahadevan, *The shape of a long leaf*, Proc. Natl. Acad. Sci. USA **106** (2009), no. 52, 22049–22054, DOI 10.1073/pnas.0911954106. MR2580802

[90] H. Liang and L. Mahadevan, *Growth, geometry and mechanics of the blooming lily*, Proceedings of the National Academy of Sciences, **108** (2011), 5516–5521.

[91] E. H. Mansfield, *The bending and stretching of plates*, 2nd ed., Cambridge University Press, Cambridge, 1989, DOI 10.1017/CBO9780511525193. MR1111482

[92] C. Maor and A. Shachar, *On the role of curvature in the elastic energy of non-Euclidean thin bodies*, J. Elasticity **134** (2019), no. 2, 149–173, DOI 10.1007/s10659-018-9686-1. MR3913889

[93] M. C. Marchetti, J-F. Joanny, S. Ramaswamy, T. B. Liverpool, J. Prost, M. Rao, and R. A. Simha, *Hydrodynamics of soft active matter*, Reviews of Modern Physics **85** (2013), no. 3, 1143.

[94] S. Müller and H. Olbermann, *Conical singularities in thin elastic sheets*, Calc. Var. Partial Differential Equations **49** (2014), no. 3-4, 1177–1186, DOI 10.1007/s00526-013-0616-6. MR3168627

[95] J. Nash, *The imbedding problem for Riemannian manifolds*, Ann. of Math. (2) **63** (1956), 20–63, DOI 10.2307/1969989. MR75639

[96] J. Nash, C^1 *isometric imbeddings*, Ann. of Math. (2) **60** (1954), 383–396, DOI 10.2307/1969840. MR65993

[97] U. Nath, B. Crawford, R. Carpenter, E. Coen, *Genetic control of surface curvature*, Science, **299** (2003), 1404–1407.

[98] S. Nechaev, *Non-Euclidean geometry in nature*, in Order, Disorder and Criticality (Yurij Holovatch editor), pp. 61–111, (2018).

[99] S. Nechaev and R. Voituriez, *On the plant leaf's boundary, "jupe à godets" and conformal embeddings*, J. Phys. A **34** (2001), no. 49, 11069–11082, DOI 10.1088/0305-4470/34/49/322. MR1872981

[100] H. Olbermann, *Energy scaling law for the regular cone*, J. Nonlinear Sci. **26** (2016), no. 2, 287–314, DOI 10.1007/s00332-015-9275-4. MR3466225

[101] H. Olbermann, *On a boundary value problem for conically deformed thin elastic sheets*, Anal. PDE **12** (2019), no. 1, 245–258, DOI 10.2140/apde.2019.12.245. MR3842912

[102] A. V. Pogorelov, *An example of a two-dimensional Riemannian metric that does not admit a local realization in E_3*, Dokl. Akad. Nauk SSSR **198** (1971), 42–43. MR0286034

[103] A. Rafsanjani and K. Bertoldi, *Buckling-induced kirigami*, Physical Review Letters **118** (2017), no. 8, 084301.

[104] P. Rodriguez, A. Hoger, and A. McCulloch, *Stress-dependent finite growth in finite soft elatic tissues*, J. Biomechanics **27** (1994), 455–467.

[105] T. Savin, N. A. Kurpios, A. E. Shyer, P. Florescu, H. Liang, L. Mahadevan, and C. J. Tabin, *On the growth and form of the gut*, Nature **476** (2011), no. 7358, 57–62.

[106] E. Sharon, B. Roman, M. Marder, G. S. Shin, and H. L. Swinney, *Buckling cascades in free sheets*, Nature **419** (2002), 579–579.

[107] E. Sharon, B. Roman, and H. L. Swinney, *Geometrically driven wrinkling observed in free plastic sheets and leaves*, Phys. Rev. E **75** (2007), 046211.

[108] E. Sharon and M. Sahaf, *The mechanics of leaf growth on large scales*, in Plant Biomechanics: From Structure to Function at Multiple Scales (Geitmann, A. and Gril, J. editors), Springer International Publishing, pp. 109–126, (2018).

[109] T. L. Shearman and S. C. Venkataramani, *Distributed branch points and the shape of elastic surfaces with constant negative curvature*, J. Nonlinear Sci. **31** (2021), no. 1, Paper No. 13, 60, DOI 10.1007/s00332-020-09657-2. MR4197392

[110] B. I. Shraiman, *Mechanical feedback as a possible regulator of tissue growth*, Proceedings of the National Academy of Sciences **102** (2005), no. 9, 3318–3323.

[111] A. E. Shyer, T. Tallinen, N. L. Nerurkar, Z. Wei, E. S. Gil, D. L. Kaplan, C. Tabin, and L Mahadevan, *Villification: how the gut gets its villi*, Science **342** (2013), no. 6155, 212–218.

[112] M. Spivak, *A comprehensive introduction to differential geometry. Vol. I*, 2nd ed., Publish or Perish, Inc., Wilmington, Del., 1979. MR532830

[113] T. Tallinen, J. Y. Chung, J. S. Biggins, and L Mahadevan, *Gyrification from constrained cortical expansion*, Proceedings of the National Academy of Sciences **111** (2014), no. 35, 12667–12672.

[114] T. Tallinen, J. Y. Chung, F. Rousseau, N. Girard, J. Lefèvre, and L. Mahadevan, *On the growth and form of cortical convolutions*, Nature Physics **12** (2016), no. 6, 588–593.

[115] H. Thérien-Aubin, Z. L. Wu, Z. Nie, and E. Kumacheva, *Multiple shape transformations of composite hydrogel sheets*, Journal of the American Chemical Society **135** (2013), no. 12, 4834–4839.

[116] D. W. Thompson, *On Growth and Form*, New edition, Cambridge University Press, Cambridge, England, 1942. MR0006348

[117] I. Tobasco, *Curvature-driven wrinkling of thin elastic shells*, Arch. Ration. Mech. Anal. **239** (2021), no. 3, 1211–1325, DOI 10.1007/s00205-020-01566-8. MR4215193

[118] I. Tobasco, Y. Timounay, D. Todorova, G. Leggat, J. Paulsen, and E. Katifori, *Exact solutions for the wrinkle patterns of confined elastic shells*, `arXiv:2004.02839`, 2020.

[119] A. M. Turing, *The chemical basis of morphogenesis*, Philos. Trans. Roy. Soc. London Ser. B **237** (1952), no. 641, 37–72. MR3363444

[120] W. M. van Rees, E. Vouga, and L. Mahadevan, *Growth patterns for shape-shifting elastic bilayers*, Proceedings of the National Academy of Sciences **114** (2017), no. 44, 11597–11602.

[121] S. C. Venkataramani, *Lower bounds for the energy in a crumpled elastic sheet—a minimal ridge*, Nonlinearity **17** (2004), no. 1, 301–312, DOI 10.1088/0951-7715/17/1/017. MR2023444

[122] W. Warner, *Topographic mechanics and applications of liquid crystalline solids*, Annual Review of Condensed Matter Physics **11** (2020), 125–145.

[123] Z. Y. Wei, Z. V. Guo, L. Dudte, H. Y. Liang, and L. Mahadevan, *Geometric mechanics of periodic pleated origami*, Physical Review Letters **110** (2013), 215501.

[124] Z. Wei, J. Jia, J. Athas, C. Wang, S. Raghavan, T. Li, and Z. Nie, *Hybrid hydrogel sheets that undergo pre-programmed shape transformations*, Soft Matter **10** (2014), 8157–8162.

[125] C. Whitewoods and E. Coen, *Growth and development of three-dimensional plant form*, Current Biology, R910-18, (2017).

[126] K. K. Yamamoto, T. L. Shearman, E. J. Struckmeyer, J. A. Gemmer, and S. C. Venkataramani, *Nature's forms are frilly, flexible, and functional*, Preprint `arXiv:2103.10509`, 2021.

[127] K. Zhang, *Quasiconvex functions,* SO(n) *and two elastic wells*, Ann. Inst. H. Poincaré Anal. Non Linéaire **14** (1997), no. 6, 759–785, DOI 10.1016/S0294-1449(97)80132-1. MR1482901

UNIVERSITY OF PITTSBURGH, DEPARTMENT OF MATHEMATICS, 139 UNIVERSITY PLACE, PITTSBURGH, PENNSYLVANIA 15260
Email address: `lewicka@pitt.edu`

SCHOOL OF ENGINEERING AND APPLIED SCIENCES, AND DEPARTMENTS OF PHYSICS, AND ORGANISMIC AND EVOLUTIONARY BIOLOGY, HARVARD UNIVERSITY, CAMBRIDGE, MASSACHUSETTS 02138
Email address: `lmahadev@g.harvard.edu`